AN ABSTRACT OF THE THESIS OF

John Merrill Brubaker for the degree of Doctor of Philosophy

in Oceanography presented on September 7, 1979

Title: Space-Time Scales of Temperature Variability in the Seasonal Thermocline of Lake Tahoe

Abstract approved: Redacted for privacy

Thermal structure in the seasonal thermocline at Lake Tahoe was investigated through the analysis of vertical temperature profiles taken in the upper 70 m during late summer stratification. Different ranges of horizontal and temporal scales were sampled in each of three subsets of finestructure profiles: (1) a three-week sequence at a midlake station, (2) a 2 1/2 hour, 12 km transect across the lake, and (3) a 2 1/2 hour sequence of intensive sampling over a 200 m transect line at midlake. The ensemble mean profile was much the same for each set, but the ensemble temperature variance, similar for (1) and (2), was smaller at all depths and distributed differently in the vertical for (3).

As a working hypothesis, it is assumed that a substantial amount of the observed temperature variability is due to internal wave displacements. Within this framework, the observations of set (3) are found to be consistent with generation by a field of small-scale internal waves obeying WKB displacement scaling. In contrast,

over the longer time scales of (1), or the larger area of (2), the dominant contribution to the variance appears to have come from a few, low order, vertical modes.

Vertical wavenumber spectra of temperature fluctuations for all three sets were similar for wavenumbers greater than about 0.1 cpm, falling as wavenumber to the -5/2 power. When interpreted as spectra of vertical displacements, the level in the 0.1 to 1.0 cpm decade was fairly constant even though the local buoyancy frequency for individual records varied from 3 to 13 cph; this spectral level was somewhat lower (by a factor of 0.3 to 0.7) than that reported for various oceanic results. WKB internal wave scaling did not improve the spectral collapse effected by the "displacement scaling" of temperature spectra. Horizontal-temporal coherence fell to 0.5, for vertical wavelengths of 13 m, at a separation of 70 m and 12 minutes. For 6.5 m wavelengths the separation was 44 m and 7 minutes.

A set of microstructure profiles was also obtained during the same project. These revealed the characteristic patchiness of microstructure activity, and the occurrence of the most intense signals in a shore-bound mixing layer over the steeply sloped bottom. With two horizontally separated thermistors on one instrument, it was determined that the shape of microscale features varied with scale, larger features being more flattened. The shape also depended on the local stratification.

Space-Time Scales of Temperature Variability in the Seasonal Thermocline of Lake Tahoe

by

John Merrill Brubaker

A THESIS

submitted to

Oregon State University

in partial fulfillment of
the requirements for the
degree of

Doctor of Philosophy

June 1980

APPROVED:

Redacted for privacy

Assistant Professor of Oceanography
in charge of major

Redacted for privacy

Dean of the School of Oceanography

Redacted for privacy

Dean of Graduate School

Thesis presented on September 7, 1979

Typed by Sherry Brubaker for John Merrill Brubaker

ACKNOWLEDGEMENTS

I am grateful for my association with Dr. Douglas Caldwell, my major professor, who always found the time for discussions and managed to make them inspiring as well as entertaining. In his (sabbatical) absence, the major professor duties were accepted by Dr. Thomas Dillon, whose support and guidance have been continuous from the outset of this project.

Dr. Victor Neal helped plan this research and brought irrepressible energy to the fieldwork. We all thoroughly enjoyed working at Lake Tahoe with Dr. Thomas Powell and his group from the University of California, Davis. Mark Matsler and Steve Wilcox built the instrumentation and helped at the lake as well. I am grateful to Dr. Murray Levine for several discussions and for the software for computing internal wave modes. Fellow graduate students Donald Denbo and Mick Spillane provided drafting assistance and software for some of the figures.

I am grateful to my parents for encouraging a healthy respect for education. And finally, I sincerely thank my wife, Sherry, for typing the thesis (except this page), but especially for making the whole Oregon experience so enjoyable.

TABLE OF CONTENTS

CHAPTER I. INTRODUCTION 1

Background and perspective. 1

CHAPTER II. FIELD PROGRAM AND DATA SETS 4

A. Physical characteristics of Lake Tahoe. 4
B. Instrumentation 9
C. Data sets 12

CHAPTER III. DESCRIPTIVE ANALYSIS OF THE FINESTRUCTURE DATA . . . 13

A. Formation of ensembles. 14
B. Ensemble (1), a three week sequence at midlake. 16
C. Ensemble (2), a cross lake-transect 23
D. Ensemble (3), intensive sampling in a local, midlake area. 29
E. Elementary ensemble statistics. 33
F. Vertical wavenumber spectra 38
G. Horizontal-temporal coherence in the local ensemble . . . 44
H. Summary 57

CHAPTER IV. INTERPRETATION AND DISCUSSION OF THE FINESTRUCTURE RESULTS 59

A. Vertical structure of internal waves. 60
B. Application to the standard deviation profiles. 64
C. Discussion of the modal interpretation. 72
D. Scaling the wavenumber spectra. 76
E. The cross spectra 83
F. Summary 86

CHAPTER V. VERTICAL MICROSTRUCTURE OBSERVATIONS 89

A. General variability 90
B. Horizontal coherence. 96
C. Summary 99

REFERENCES 102

LIST OF ILLUSTRATIONS

Figure		Page
II.1	Map of Lake Tahoe, California-Nevada	5
III.1	Temperature profiles in the three-week set (E-1)	17-18
III.2	Heat content and average temperature versus time for several depth intervals in E-1	21
III.3	Temperature profiles in the transect set (E-2)	25
III.4	Isotherm contours along the transect	28
III.5	Sampling station grid for the local ensemble (E-3)	30
III.6	Horizontal variability of a thin, mixed layer at 25 m depth	32
III.7	(a) Ensemble mean and standard deviation temperature profiles for the station ensemble (E-1)	34
	(b) As in (a), but for the transect (E-2)	35
	(c) As in (a), but for the local ensemble (E-3)	36
III.8	(a) Buoyancy frequency, N(z), for the station ensemble (E-1)	39
	(b) As in (a), but for the local ensemble (E-3)	40
III.9	Vertical wavenumber spectra of temperature fluctuations for all three ensembles over the depth range 15 to 66.1 m	42
III.10	(a) Short-interval temperature spectra at four depths for the station ensemble (E-1)	46
	(b) As in (a), but for the local ensemble (E-3)	47
III.11	Coherence and phase spectra, with pair separation as a curve parameter	50
III.12	Coherence and phase, plotted against separation, for two values of the vertical wavenumber	52
III.13	Correlation map for variability about a polynomial trend over the depth range 15 to 40.5 m	55

List of Figures (continued)

Figure		Page
IV.1	(a) Ensemble standard deviation displacement profile for the station ensemble (E-1)	66
	(b) As in (a), but for the local ensemble (E-3)	67
IV.2	Profile of WKB-scaled displacements for the local ensemble (E-3)	69
IV.3	Three lowest order vertical modes for the vertical displacement wavefunction at a 12-hour period.	71
IV.4	Root-mean-square vertical displacement profile due to random-phase realizations of the three 12-hour modes, superimposed on the ensemble displacement profile of E-1.	73
IV.5	(a) Displacement spectra for E-1, formed from the temperature spectra of Figure III.10 (a)	78
	(b) As in (a), but for E-3 (cf. Figure III.10(b))	79
IV.6	(a) WKB-scaled spectra for E-1	81
	(b) As in (a), but for E-3	82
V.1	Microstructure drop 2-F, illustrating general vertical variability of small-scale variance	91
V.2	Microstructure drop 9-D, a "quiet" record in which virtually all the microstructure is positive (stable gradients)	93
V.3	Microstructure 5-B, showing the penetration of mixing activity due to surface forcing	94
V.4	Microstructure drop 15-D. Increased microstructure level due to slope-induced mixing. The temperature profile shows that the thermocline here is composed of a series of mixed layers of varying thicknesses, separated by high-gradient sheets.	95
V.5	Aspect ratio versus depth for three horizontal separations.	98
V.6	Mean aspect ratio in the depth interval 20 to 50 m as a function of separation	100

LIST OF TABLES

Table		Page
II.1	Morphometric parameters of Lake Tahoe, Crater Lake, and Lake Michigan	6
III.1	Sampling information for the ensembles	15
III.2	Heat content changes over the station ensemble (E-1)	24
III.3	Mean gradient and buoyancy frequency for the short-interval spectra shown in Figure III.10	45
III.4	Pair groups drawn from the local ensemble (E-3), used in cross-spectral analysis	49

SPACE-TIME SCALES OF TEMPERATURE VARIABILITY IN THE SEASONAL THERMOCLINE OF LAKE TAHOE

CHAPTER I. INTRODUCTION

Motions and structures in geophysical fluids are known to occur over an enormous range of space and time scales, reflecting a variety of physical processes and dynamic balances. The focus of this investigation is on relatively small vertical scales in the temperature field of a natural, freshwater lake, and on the horizontal and temporal variability of these thermal structures. Specifically, the objectives of this work are to characterize and, when possible, to interpret temperature finestructure and microstructure observations made with vertical profiling instruments in the upper thermocline of Lake Tahoe during late summer stratification.

Background and perspective.

The motivation for studying small-scale phenomena is clear and strong: they are ubiquitous, they are not well understood, and they play a key role in the general science of geophysical fluids.

With advances in oceanographic instrumentation came reports of variability in (for example) temperature down to the smallest resolvable scales. "Microstructure" appeared in the oceans (Cooper and Stommel, 1968; Tait and Howe, 1968), under an Arctic ice island (Neal, Neshyba, and Denner, 1969) in the Mediterranean Sea (Woods

and Wiley, 1972) and in freshwater lakes (Simpson and Woods, 1970; Neal, Neshyba, and Denner, 1971 ; Lazier, 1973).

The freshwater work illustrates a point that is, we hope, relevant to the present study, namely, that observational programs in lakes can be invaluable in clarifying the physics of natural waters when combined with results of oceanic research. For instance, in the early days of microstructure, when speculations as to its origin were first offered, a fascinating one among them involved the dependence of density on two fluid properties (heat and salt) with different molecular diffusivities. Double-diffusive convection phenomena (Turner, 1973) can occur when the gradient of one property is stabilizing while the gradient of the other is destabilizing, the overall density gradient being statically stable. Such convection can produce microstructure in the ocean under the proper conditions, and Williams (1975) has made direct observations of it, but the work of Simpson and Woods (1970) and Neal, Neshyba, and Denner (1971) showed that other mechanisms in stratified fluids can generate similar microstructure in the absence of a salinity gradient.

Research in a freshwater lake by Lazier (1973) is generally recognized as the first evidence that small-scale temperature fluctuations could be due entirely to the transient distortion of the mean temperature field by internal wave displacements. This result has been of considerable importance in oceanic internal wave studies, and it plays a central role in the present work.

The lack of understanding of small-scale processes has an impact on investigations of large-scale phenomena. Holland (1977) stresses repeatedly that the inability to parameterize adequately the small-scale mixing represents a great impediment to progress in development of general circulation models for the oceans.

The upper thermocline, the domain of this study, is a very active and complex environment. Even in the presumably simpler deep ocean, the structure and dynamics of internal waves and mixing are only partially understood, although considerable progress has been made (Garrett and Munk, 1979). Results for the upper thermocline are less extensive, although Pinkel (1975) has presented a nice analysis of a very large set of temperature profiles taken from the research platform Flip. The present study represents a further contribution toward the understanding of small-scale phenomena in the strongly stratified upper thermocline setting.

The semantics of this field have not been consistent over the past decade; usage in this thesis is as follows. "Finestructure" refers to variability resolved by the TD (temperature-depth) profiler, i.e. vertical scales down to tens of centimeters. "Microstructure" here refers to the smaller vertical scales resolved by the MSP (microstructure profiler), which are of the order of one centimeter, but depend on the noise level. The instruments are described in Chapter II.

CHAPTER II. FIELD PROGRAM AND DATA SETS

A. Physical characteristics of Lake Tahoe.

Tahoe is usually described as a large, deep lake, presumably in the context of the global distribution of basin sizes. Specifically, Hutchinson (1957) lists its area as 499 km^2 and maximum depth as 501 m (tenth deepest known lake at that time). Although the mean depth, defined as the ratio of the volume of the lake to its area, is 249 m, one can see from Figure II.1 that there is a large, flat, almost rectangular portion over 400 m deep, bounded along most of its perimeter by steep slopes. This is characteristic of the basin's tectonic origin as a down-faulted trough (graben). For comparison, morphometric parameters of Crater Lake and Lake Michigan are listed in Table II.1 along with those of Lake Tahoe. The basin is located on the California-Nevada border at 39° 09'N, 120° 08'W; the average summertime lake level is 1898 m (6226 ft) above mean sea level (National Ocean Survey chart no. 18665).

As a popular resort area, Lake Tahoe has been subjected to increasing environmental pressure (Goldman, 1970) but the water has, so far, retained a striking beauty and clarity. A quantitative optical characterization was presented by Smith et al. (1973), partly as baseline information with which to judge possible future deterioration. They measured (in winter) a beam attenuation coefficient of 0.187 m^{-1}, comparable to very clear oceanic water,

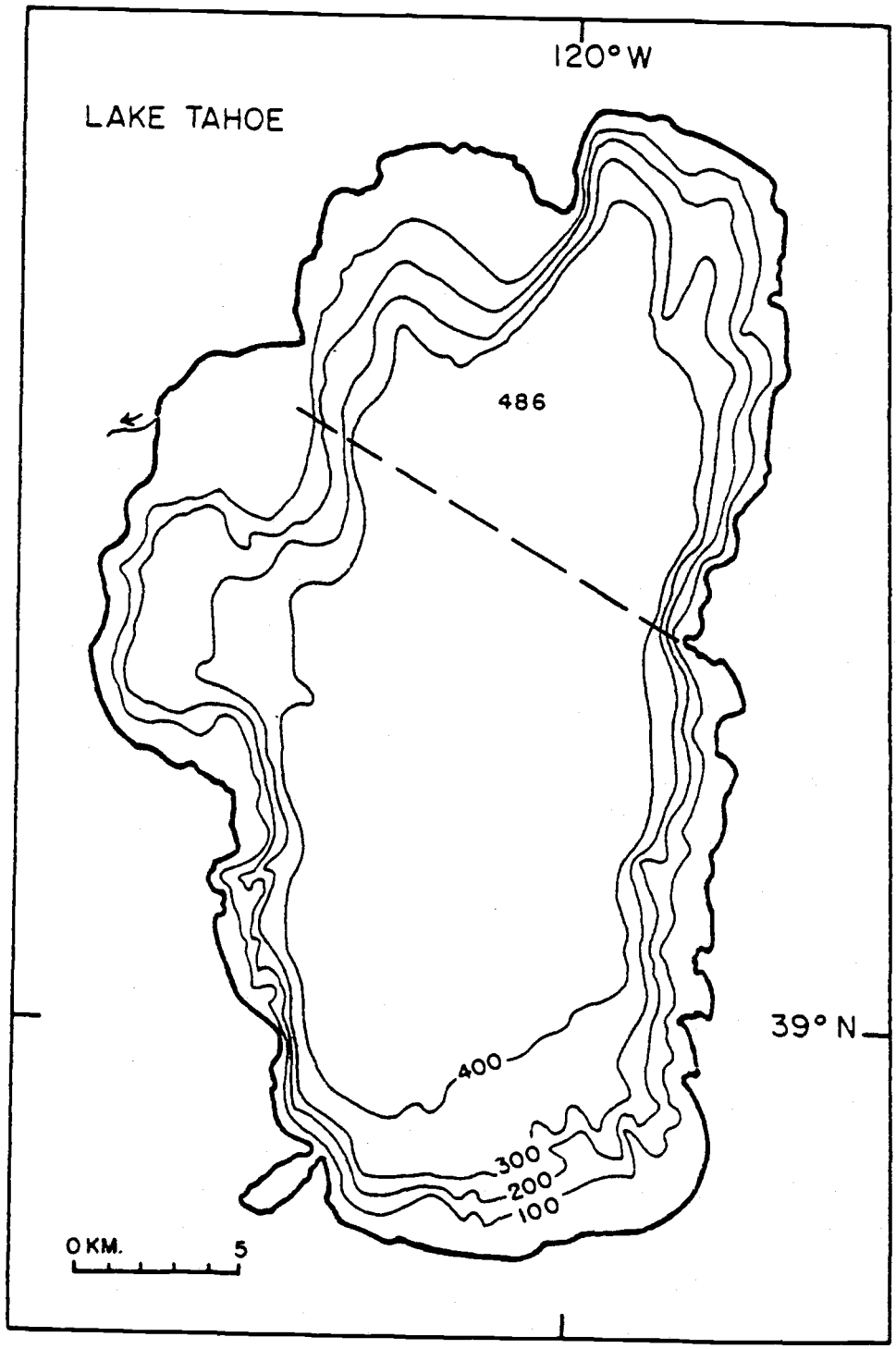

Figure II.1 Map of Lake Tahoe, California-Nevada (based on National Ocean Survey Chart No. 18665). Depth contours are in meters. The dashed line indicates the trackline of the cross-lake transect (Section III.C).

TABLE II.1 Morphometric parameters of three North American lakes.

	Tahoe	Crater	Michigan
Area, km^2	499	55	57,850
Max. depth, m	501	608	265
Mean depth, m	249	364	99
Volume, km^3	124	20	5,760

Data from Hutchinson (1957)

but they note that some natural waters, for example the Sargasso Sea (and, they suspect, Crater Lake) have even lower values, i.e., they are more transparent. In the same paper, Secchi disk observations over four and a half years are summarized, revealing a seasonal cycle. In midwinter, the average Secchi disk depth was about 33 m; in August it was about 25 m. Discussing the range of Secchi depths in lakes, Hutchinson (1957, p. 403) notes that values over 30 m are very rare. Finally, Smith, et al. (1973) report a winter value of 0.058 m^{-1} for the attenuation coefficient for total irradiance. We may conclude that the water of Lake Tahoe is unusually clear.

Several factors can influence the large-scale dynamics of geophysical fluids. Coriolis effects due to the rotation of the earth, density stratification, and length scales imposed by boundaries may be important (Pedlosky, 1971). For example, all three effects influence a nondimensional parameter relevant to the present work, $r = fL/c$, where f is the Coriolis parameter, L is a horizontal basin scale, and c is the horizontal phase speed of long waves. This quantity may be regarded as a nondimensional basin width (Csanady, 1975) where the actual width has been scaled by the Rossby radius of deformation, c/f. It is also a ratio of two time scales: the time for a disturbance to propagate across the lake, L/c, and the inertial time scale, f^{-1}. In any case, the magnitude of r indicates the relative importance of rotation.

In the surface or barotropic mode (the only possible mode when the lake is homogeneous), $c^2 = gh$, where g is the acceleration of gravity and h is the water depth. Using h = 450 m, the phase speed is 66.4 m/s. At 39°latitude, $f = 9.15 \times 10^{-5}$ rad/s and we may use L = 15 km as a characteristic basin width (at roughly half depth). Thus, r = 0.02 and, in this mode, Tahoe is "small." Surface seiches will be modified negligibly by rotational effects.

When the water is stratified, additional vertical modes may be present. For these internal, or baroclinic, motions the phase speed is much less than in the surface mode, a typical value being 0.34 m/s (see section C in Chapter III). The corresponding r is 4, indicating a considerable rotational influence.

Some appreciation for this effect comes from consideration of Kelvin wave amplitudes, which fall off as exp(-fx/c) with distance, x, from shore. Mortimer (1974) has arbitrarily defined a "narrow" lake as one across which the amplitude of a Kelvin wave decreases by less than 5%. If the attenuation is between 5% and 95%, the width is "medium," and if it is greater than 95%, the width is "large." In this classification, the width of Lake Tahoe is narrow for a surface Kelvin wave (2% amplitude decrease) and large for an internal Kelvin wave (98% decrease). However, there is still an important distinction to be drawn between Lake Tahoe and basins the size of the Great Lakes, with widths of order 100 km. For the latter, the (internal) Kelvin wave amplitude becomes negligible at a distance of two or three deformation radii from shore (say 10

or 15 km), which is well under half the total width. Thus, Kelvin waves and associated effects are of a boundary layer nature, separate from the general interior of the lake. Csanady (1972) has studied these phenomena theoretically in a circular lake model and the results have been extended and applied with some success in interpreting some observations in Lake Ontario (Csanady and Scott, 1974). Since Lake Tahoe is only three or four deformation radii in total width, the boundary layer characterization is not appropriate.

B. Instrumentation.

Vertical temperature profiles, the principal data for this study, were obtained with two totally different instrument systems: 1) a temperature-depth (TD) recorder, and 2) a microstructure profiler (MSP).

The TD was so named because of operational similarity to the CTD (conductivity-temperature-depth) instrument, a staple in oceanographic research. Both are winch-lowered by taut cable, thus coupling the sensor to the motion of the vessel. Under our usual operating conditions, the boat motion was small and vertical resolution was actually limited as much by the system least count (see below).

Design of the TD was dictated by requirements of simple, rapid, reliable sampling with real-time graphical output directly interpretable in physical units for temperature and depth. In

fact, the reason for having the TD was that the MSP did not meet most of the listed requirements and an auxiliary instrument was needed for quick temperature surveys and background data. As it turned out, the TD played much more than a supporting role, providing data of interest in its own right.

The temperature sensor was a Thermometrics P-85 bead thermistor with frequency response characterized by -3 db power attenuation at approximately 8 Hz. A strain gauge type pressure transducer provided the depth signal. In the overboard unit, the signals were pre-amplified, and then sent up conductors in the winch cable, through slip rings, to onboard gain-offset amplifiers and finally to a Hewlett Packard XY recorder.

For analysis beyond visual inspection, the traces were digitized at 0.01 inch intervals with a Calma digitizer which wrote the data onto computer-compatible magnetic tape. Least count values were 0.1 m for depth and about 0.02 ^{o}C for temperature. Allowing for some operator error in the digitization, the overall uncertainty in the data is reckoned to be two or three least counts.

The MSP used at Lake Tahoe was similar in concept to one described by Caldwell, Wilcox, and Matsler (1975) using simple PVC construction, low power electronics immersed in freon at in situ pressure, and helicopter type wings. The fall rate can be controlled by adjusting buoyancy and wing angle; at Tahoe, speeds from 4 to 30 cm/s were used. Since that paper was written, some significant improvements were made in time for the present field work.

The data link and recovery line were combined into a single 1.6 mm diameter cable composed of: four pairs of conductors (XBT wire), a surrounding sheath of Kevlar fiber for mechanical strength, and a coating of syntactic foam. The cable must always be kept slack during a profile to allow the probe to fall as freely as possible; the purpose of the foam is to prevent the loose line from drooping over the instrument and fouling in the wings.

The temperature sensor used with the MSP was the P-85 thermistor and the pressure transducer was the wire-wound variable resistance type (solid state pressure sensors have been used on post-Tahoe units and have been found to be superior). The amplified temperature signal was sent directly (i.e. not encoded) up the data link. Onboard analog signal processing included, in order: a gain-offset stage, a 6-pole Butterworth filter (-3 db at 30 Hz), a differentiator with adjustable gain, and another 6-pole filter. The final output was digitized at (typically) 80 samples per second, the pre-differentiator signal at half that rate. The pressure signal was sent by frequency modulation (FM) transmission, discriminated onboard, and sampled at 1/16 the rate of the final, differentiated temperature. All digitized signals, along with time base data and system test words, were written directly onto computer-compatible magnetic tape at acquisition time.

Both temperature systems were deployed from a 25 foot houseboat. Power (120 VAC) was supplied either by a bank of 12 VDC

storage batteries connected to an inverter, or by a gasoline engine Honda generator with separate voltage regulator.

C. Data sets.

Aside from occasional references to the current meter results of Dillon and Powell (1979), this investigation is based on selections of TD and MSP profiles taken during September, 1976, over a period of about three weeks. Most profiles were taken at a midlake station east of Ward Creek. Marker buoys were in place there and those served as a reference for our position. However, except for the "local" ensemble, discussed in detail in Chapter III, no attempt was made to establish our position more precisely than to estimate it as within about 1 km of the buoys.

On two occasions, profiles were obtained near the northwest shore, over the steeply sloped bottom. Some results from those measurements appear elsewhere (Caldwell, Brubaker, Neal, 1978); additional discussion is given in Chapter V, which deals with microstructure observations.

The TD profiles cover the upper 70 m, the MSP profiles about 95 m. At least 90% of the temperature drop from, typically, 16 ^{o}C in the mixed layer to an assumed bottom temperature of 4.5 ^{o}C occurs within the upper 70 m.

CHAPTER III. DESCRIPTIVE ANALYSIS OF THE FINESTRUCTURE DATA

Each TD profile provides a one-dimensional view of the temperature structure in the upper 70 m; the entire set of profiles encompasses a wide range of time and horizontal length scales as well. In this chapter, the emphasis is on an objective characterization of the observed space-time variability without explicit regard for the underlying processes that generated it. Interpretation of the results will be taken up in the next chapter.

Naturally, the strength of the profiler as an observational tool lies in the vertical resolution it provides compared to, for example, typical moored or towed instruments. In trade, one sacrifices resolution in the temporal and horizontal dimensions, sampling them through groups of profiles. The grouping is an important feature of the present work. Three ensembles of fine-structure profiles were formed, and widely different ranges of horizontal and temporal scales were represented in each.

The first part of this chapter is devoted to sampling considerations for the ensembles, and generally qualitative descriptions of their variability. Beginning in Section E, the presentation becomes quantitative, dealing primarily with perturbations about the ensemble mean profile of each of the three sets.

A. Formation of ensembles.

With only one instrument it is impossible, of course, to obtain the set of simultaneous profiles required for a strictly synoptic view of the spatial temperature structure. Likewise, given practical limitations on position fixing and holding, along with changes at one position due to currents and current shear, it is clearly impossible to restrict a sequence of profiles to purely temporal effects. We can't, therefore, separate completely the temporal from the horizontal variability, but we can at least compare characteristics of ensembles covering very different ranges of time and horizontal length.

Constrained by operational requirements of fairly calm weather and daylight hours, and sharing the usable conditions among several measurement programs, the sampling pattern for the TD data turned out to be somewhat irregular, but was, nevertheless, well suited for the grouping of profiles into sets representing three different combinations of time and horizontal length scales. Table III.1 summarizes the sampling in each ensemble.

Ensemble (1) spans the entire period of the (midlake) TD data set, almost three weeks. There is no systematic spatial pattern to this set, but all of the profiles were taken within a 1 km radius of midlake moorings, i.e. "on station." In ensemble (2), the entire basin width was sampled as rapidly as possible in a cross-lake transect, reversing the space-time proportions of ensemble (1). Intensive, organized sampling produced ensemble (3) which covers

TABLE III.1. Sampling information for the ensembles.

Ensemble Designation	Number of profiles	Horizontal		Time	
		Interval	Span	Interval	Span
Station (E-1)	21	*	*	2h-4 days	19 days
Transect (E-2)	14	0.7-1. km	11.5 km	7-19 min.	145 min.
Local (E-3)	30	30 m	200 m	5 min.	155 min.

*All profiles taken at same nominal location.

an area at midlake comparable to that of (1) over a time span comparable to that of (2).

B. Ensemble (1), a three-week sequence at midlake.

The distribution in time of the midlake profiles was very uneven so some selection criterion had to be established to produce a more uniform time sequence. This was the scheme employed: the first and last midlake profile of each sampling day were selected. If they were separated by less than two hours, only the first was kept (and on some days only one profile was made). The resulting collection is presented in Figure III.1 where the profiles are offset according to the day they were taken (two profiles from the same day being superimposed). Obviously, this sequence is still non-uniform in time, but no one day is unfairly weighted.

In the top few meters of water, the temperature structure is highly variable and strongly coupled to external forcing by solar radiation and local winds. On 9 September, for example, with virtually no wind in the time between the two profiles plotted (0915 and 1628 Pacific Daylight Time, PDT) a very shallow, high-gradient thermocline formed separating surface water, several degrees warmer, from the rest of the epilimnion. But on the 12th, light afternoon winds had stirred the day's thermal input down a little deeper and reduced the interfacial temperature difference by the time the last profile was taken that day at 1611. The field program was not designed to investigate the very near surface

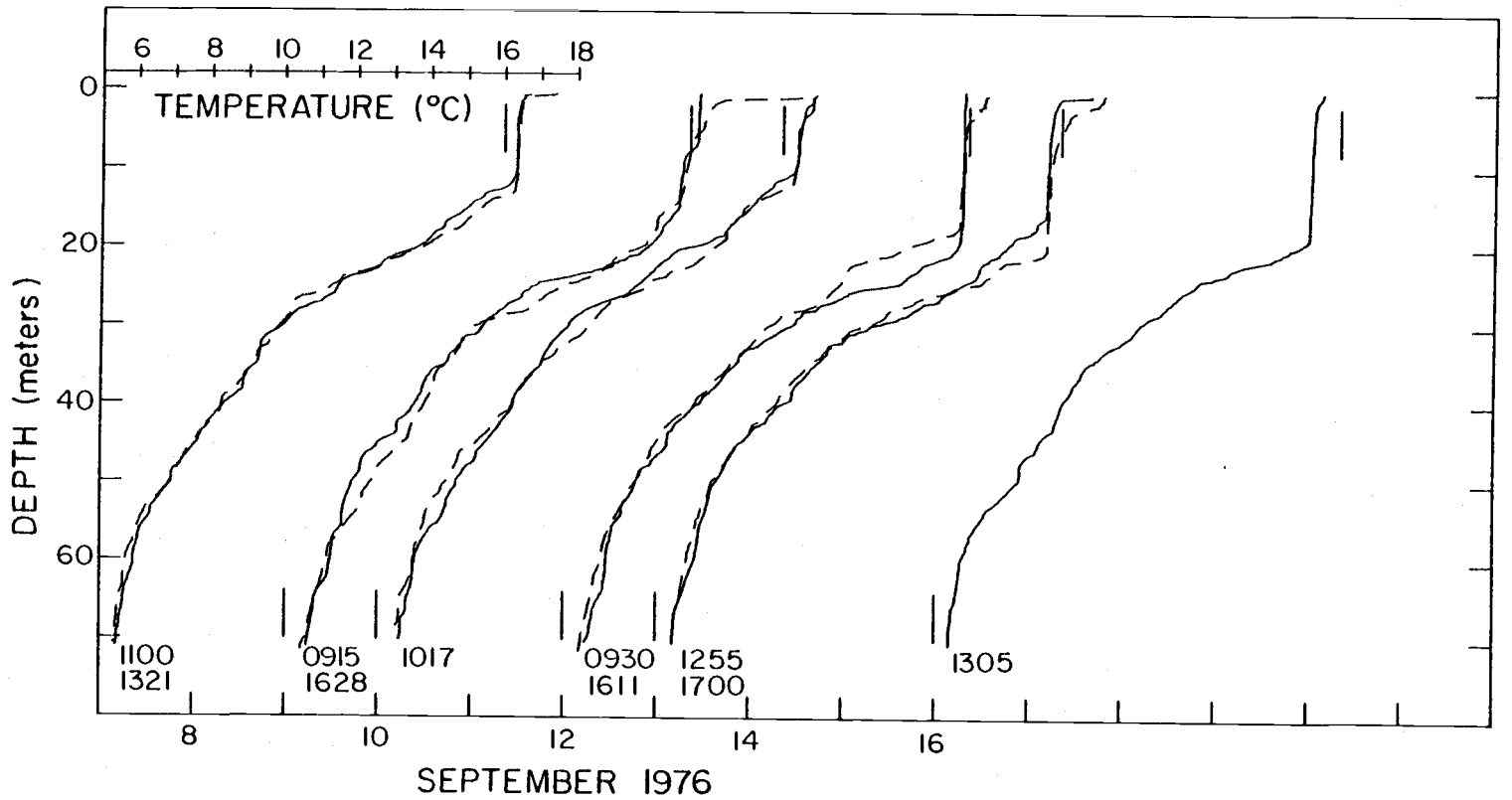

Figure III.1 Temperature profiles in the three-week set (E-1). Temperature scale applies to far left profile. Short vertical lines at the bottom and top of each profile represent 5 and 16 °C respectively. Times (PDT) are noted at the bottom of each profile (dashed curve represents later profile). Position of the 5 °C reference line with respect to the bottom axis indicates the day the profile was taken. (Continued on next page)

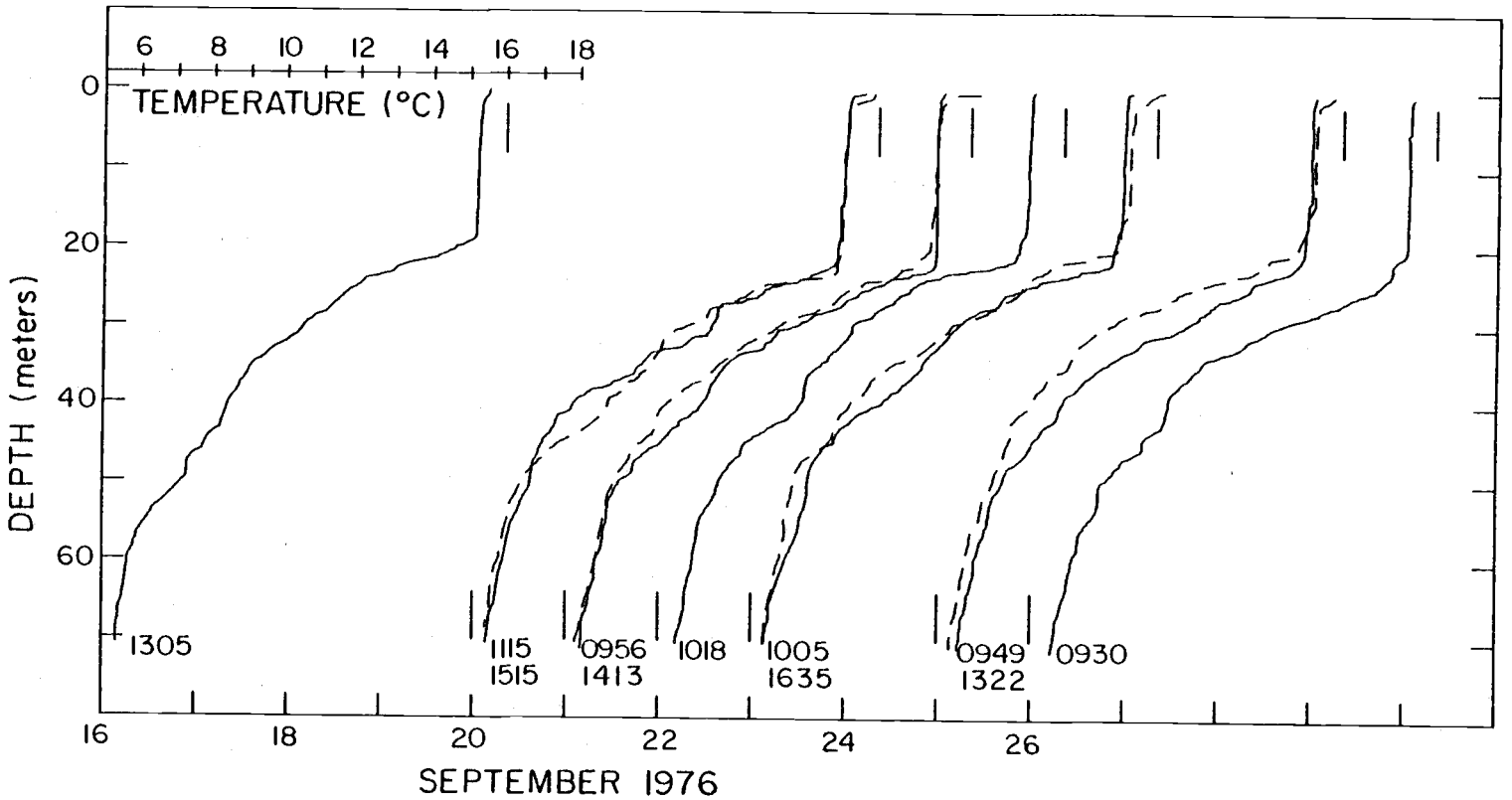

Figure III.1 (continued)

response or the details of air-water interaction quantitatively, but the variety and evolution of observed structures throughout the entire data set suggest a direct surface forcing and rapid response in the top several meters of water.

Less dramatic than the near-surface variability, but more substantial energetically, are the changes in the thickness and temperature of the epilimnion or "mixed" layer. The existence of a discernible mixed layer in nearly every profile implies that in the equilibrium balance, at least for time scales longer than a few days, sufficient energy for mixing is available that the extent of restratification is severely limited. Probably, this is true as well for much shorter time scales but the data of 9 September exemplify the occasional dominance of buoyancy effects and the development of significant vertical gradients.

Mixed layer changes through September appeared to occur more as events than as steady processes. The first major change, between 10 and 12 September, involved several meters of deepening and nearly a degree of cooling. Further cooling between 13 and 16 September brings the mixed layer to a state that remains fairly steady for the next 10 days.

In the thermocline, considerable temperature variability is apparent over time periods separating the two profiles of the same day. On 20, 21, and 23 September, relatively large fluctuations occurred between 35 and 50 m. On the 22nd, although there is only one profile, the same depth interval appears to contain the same sort

of perturbation. By contrast, on the 25th the large temperature changes were not so localized vertically.

Whether a long-term trend underlies the thermocline variability is unclear from Figure III.1. Another perspective can be obtained by looking at an integrated quantity, the heat content (per unit area) of a layer defined by

$$H(z_1,z_2) = \rho c_p \int_{z_1}^{z_2} (T(z) - T_r)dz$$

where ρ is the water density, c_p is its specific heat, $T(z)$ is the temperature at depth z (taken as positive downward), T_r is a reference temperature, and z_1 and z_2 are the depths at the top and bottom of the layer. Numerical values of $\rho = 1$ g cm^{-3}, $c_p = 1$ cal g^{-1} ^{o}C^{-1}, and $T_r = 4$ ^{o}C were used for all heat content calculations.

The heat content of the interval from 5-65 m, and that of each 10 m sub-interval, were computed for each of the profiles of this ensemble. The results are shown in Figure III.2 (for days having two profiles, their mean is plotted). Note that the mean layer temperature

$$\overline{T} = (z_2 - z_1)^{-1} \int_{z_1}^{z_2} T(z)dz$$

is simply related to the heat content by

$$\overline{T} = T_r + H/(\rho c_p(z_2 - z_1))$$

and is also indicated in Figure III.2.

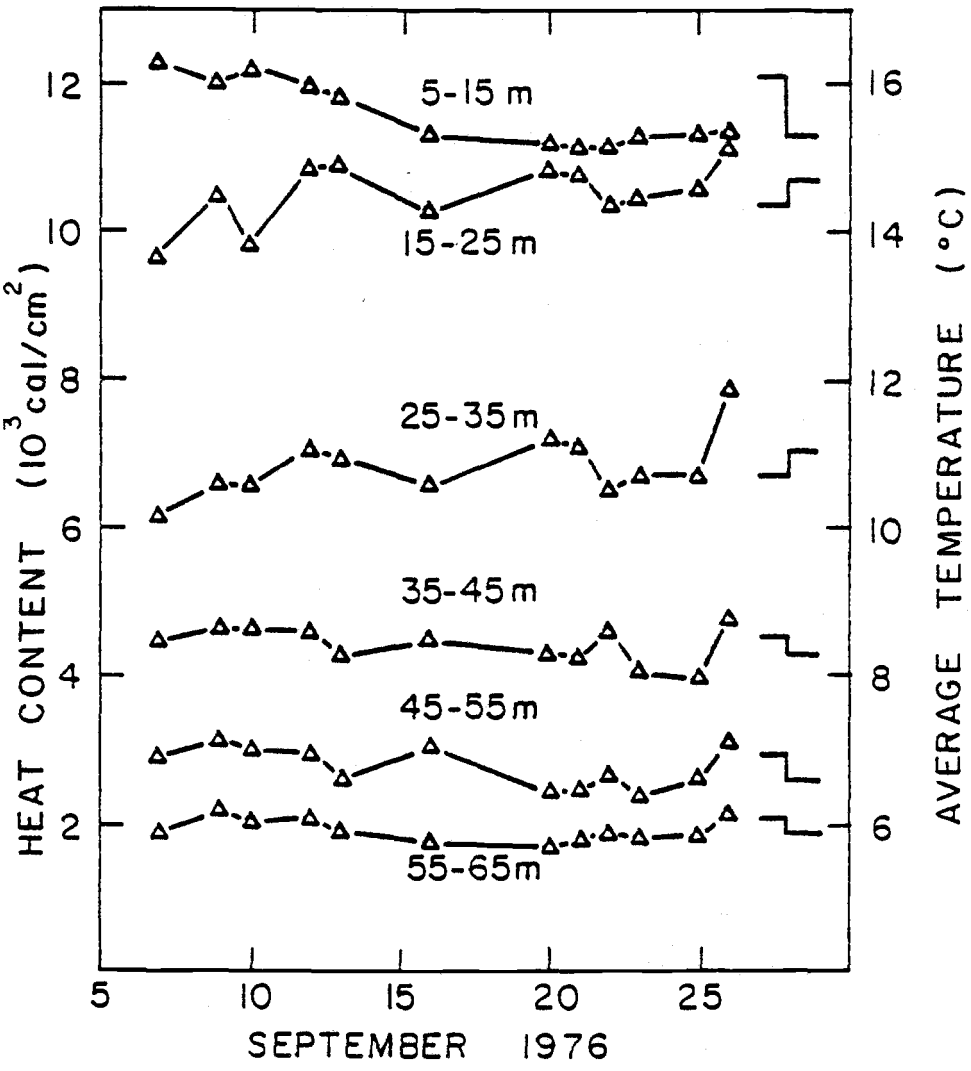

Figure III.2 Heat content and average temperature versus time for several depth intervals in E-1. The two-step symbol to the right represents the averages for the early and late weeks.

The evolution of the 5-15 m interval, which is always in the mixed layer, is rather more simple than that of the other 10 m layers, its main feature being the heat loss between 13 and 16 September. The 15-25 m interval, containing the mixed layer-thermocline transition, and the 25-35 m interval exhibit more short-term variability and less long-term trend than their shallower counterpart. The three lower intervals are again, perhaps, smoother in the short term although part of this is due to the effectiveness of daily averaging in filtering out the fluctuations between 35 and 50 m that are so plain in Figure III.1.

On seasonal time scales, large quantities of heat are exchanged between the lake and the atmosphere and are transported up or down the water column. Hutchinson (1957) gives the annual heat budget for Lake Tahoe as 34,800 cal cm^{-2}; this is the difference between its maximum and minimum heat content over the yearly cycle. September is a transitional month from the summer heating period to the fall regime of cooling and mixing. To determine whether significant net changes took place over the measurement period, one might do a linear least-squares regression of heat content against time for the various layers to obtain the slope value, with confidence interval, as a measure of the general trend. However, of the 21 profiles in this set, 10 are from the first week, 10 from the last week, and only one from the middle week. It seemed more appropriate for these data, to group the first 10 profiles into one set, the last 10 into another, and examine the difference

in mean heat content between the two sets.

The results appear in Table III.2 along with the probability of obtaining a difference of the observed magnitude, if in fact the true means of the late and early groups were equal. The early and late levels of heat content (or average layer temperature) are also illustrated in Figure III.2 by the symbol on the right. Between 15 and 35 m, some warming occurred, although the large fluctuations among profiles for these layers make this an uncertain result. All the other layers cooled, and by an amount more significant compared to their "noise." The small magnitudes of these trends confirm this September's status as a transitional period in the seasonal heating and cooling cycle.

C. Ensemble (2), a cross-lake transect.

On 10 September 1976, a series of temperature profiles was taken along a line connecting the Lake Forest Coast Guard pier on the west shore with Deadman Point on the east (see Figure II.1). From these, a subset was selected with fairly uniform horizontal spacing to represent the cross-lake variability. Sampling information is in Table III.1, and the profiles themselves are shown in Figure III.3.

There is the inevitable space-time ambiguity to the observed variability. Since horizontal currents will advect thermal structures (if there are horizontal temperature gradients) and internal waves will cause temperature perturbations associated

Table III.2. Heat content changes for 10 m layers from the early week to the late week of the Station ensemble, E-1. Standard errors are shown with the means.

Depth interval (m)	Mean heat content Early (cal/cm^2)	Mean heat content Late (cal/cm^2)	Difference (cal/cm^2)	Probability of equal means
5-15	12066±58	11248±28	-818	$<10^{-23}$
15-25	10363±196	10689±88	326	0.13
25-35	6698±112	7020±179	322	0.13
35-45	4552±54	4288±138	-264	0.08
45-55	2969±77	2594±81	-375	8.2×10^{-4}
55-65	2049±42	1877±48	-172	0.01

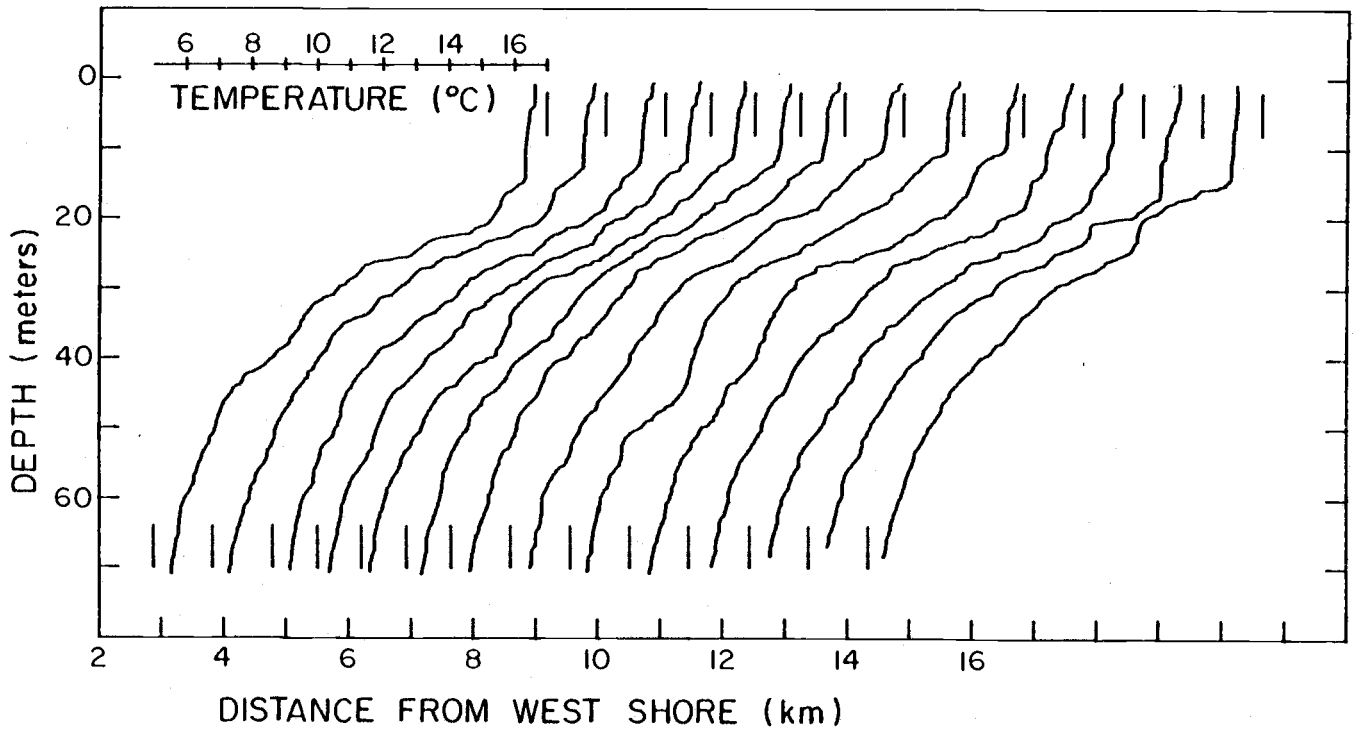

Figure III.3 Temperature profiles in the transect set (E-2). Temperature scale applies to far left profile. Short vertical lines at the bottom and top of each profile represent 5 and 17 ^{o}C respectively. Position of the 5 ^{o}C reference line with respect to the bottom axis indicates the location of the profile along the transect.

with their displacements to propagate through the water, we should compare typical speeds of these phenomena with the sampling speed. At a midlake mooring, Dillon and Powell (1979) observed currents in the upper 26 m during September 1976 that rarely exceeded 0.1 m/s. A convenient speed scale for internal waves may be obtained by representing the gross features of stratification with a two-layer model (Lamb, 1945). With the lower layer much thicker than the upper, clearly true for Lake Tahoe, the phase speed of long waves on the interface is given by $c^2 = \alpha \Delta T g h$, where α is the coefficient of thermal expansion ($-6 \times 10^{-5}\ ^{o}C^{-1}$ at mid-thermocline), ΔT is the temperature difference between the lower and upper layers ($-10\ ^{o}C$), g is the acceleration of gravity (9.8 m/s^2) and h is the upper layer thickness (20 m), giving c = 0.34 m/s. In Chapter IV, where internal wave properties are computed for the actual (i.e. not two-layer) stratification and the effects of rotation are included, we will see that this wave speed is indeed representative. A speed characterizing the sampling may be defined as the average inter-station spacing divided by the average time interval: 0.88 km/11 min = 1.31 m/s.

Thus, the effects of advection and wave propagation should be relatively minor. There is still the uncertainty of the relative importance of purely temporal changes occurring in the time involved in making the transect. Some perspective will be acquired later in this chapter when the variability of this ensemble can be compared with that of the "local" ensemble which spanned an equal

time period. It must be concluded that the larger variance in the transect ensemble is associated with its larger horizontal extent. Qualitatively, this may be seen by comparing the variety of profile shapes in Figure III.3 with the two profiles on 10 September (the transect day) in Figure III.1, separated by two hours.

Assuming, then, that this ensemble does represent large-scale horizontal variability, we may pick out some features of the cross-lake structure in Figure III.3. There is, in addition to random looking changes in the thermocline, a somewhat systematic thinning of the epilimnion from west to east, probably associated with large scale internal waves. The abrupt change of mixed layer character in the four eastern-most profiles indicates a boundary effect. Isotherm contours are shown in Figure III.4 based on all the transect profiles, including some more closely spaced ones near the west coast that are not part of the so-designated transect ensemble. The shape of the 16 ^{o}C isotherm indicates the tilt of the mixed layer base, but deeper, the cross-lake structure is more complex. It appears that the horizontal length scale associated with isotherm displacements decreases with depth. However, the magnitude of these vertical displacements about the isotherm's mean depth is on the order of a few meters, independent of depth or horizontal scale.

Within the most strongly stratified part of the thermocline, say from 15 to 11 ^{o}C, cross-lake variations were vertically coherent in general. In contrast, below about 30 m the isotherm fluctuations

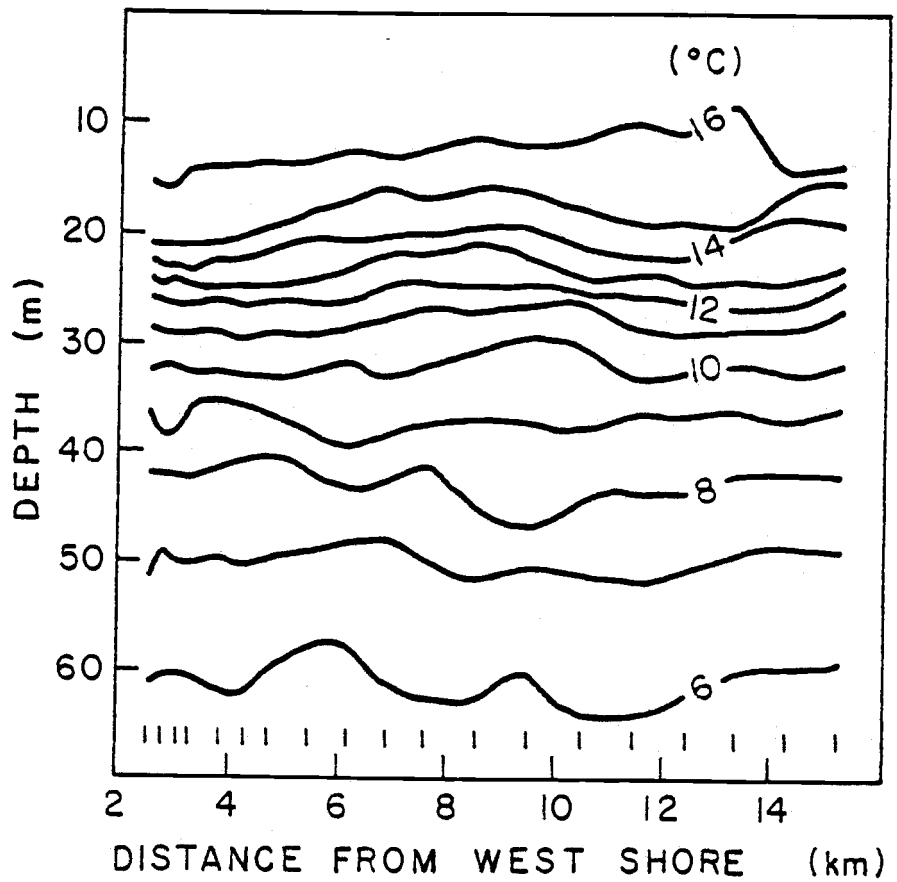

Figure III.4 Isotherm contours along the transect. Short vertical lines above the distance scale indicate the location of profiles along the transect.

appear to be less correlated or, indeed (and this may just be coincidence), negatively correlated as appears to be true for the 6 and 8 ^{o}C isotherms and perhaps 8 and 10 ^{o}C as well. Again, these comments apply only well away from the coasts.

D. Ensemble (3), intensive sampling of a local, midlake area.

On 7 September 1976, a sequence of temperature profiles was obtained with the following sampling procedure: beginning at a midlake marker buoy, a profile was taken every five minutes while the boat drifted freely. After four to eight such casts, the boat was quickly returned to the buoy and another transect was begun. Winds were extremely light but steady during the measurement period (1100-1335 PDT), causing the boat to drift an estimated 30 m each five minutes (10 cm/s or 0.2 kt). The resulting sampling grid is shown in Figure III.5. The first and last profiles at the buoy, numbers 4 and 30, are also members of ensemble (1) and are plotted in Figure III.1.

Given our unsophisticated navigation and the usual complications of currents and waves, the question of just what has been sampled again deserves some attention. Since the current meter mooring (Dillon and Powell, 1979) was not deployed this day, no direct measurements are available, but if currents or waves were running at the speeds discussed in the previous section their influence on the sampling interpretation would be critical. However, a feature in the thermal structure was observed which has some bearing on the sampling question.

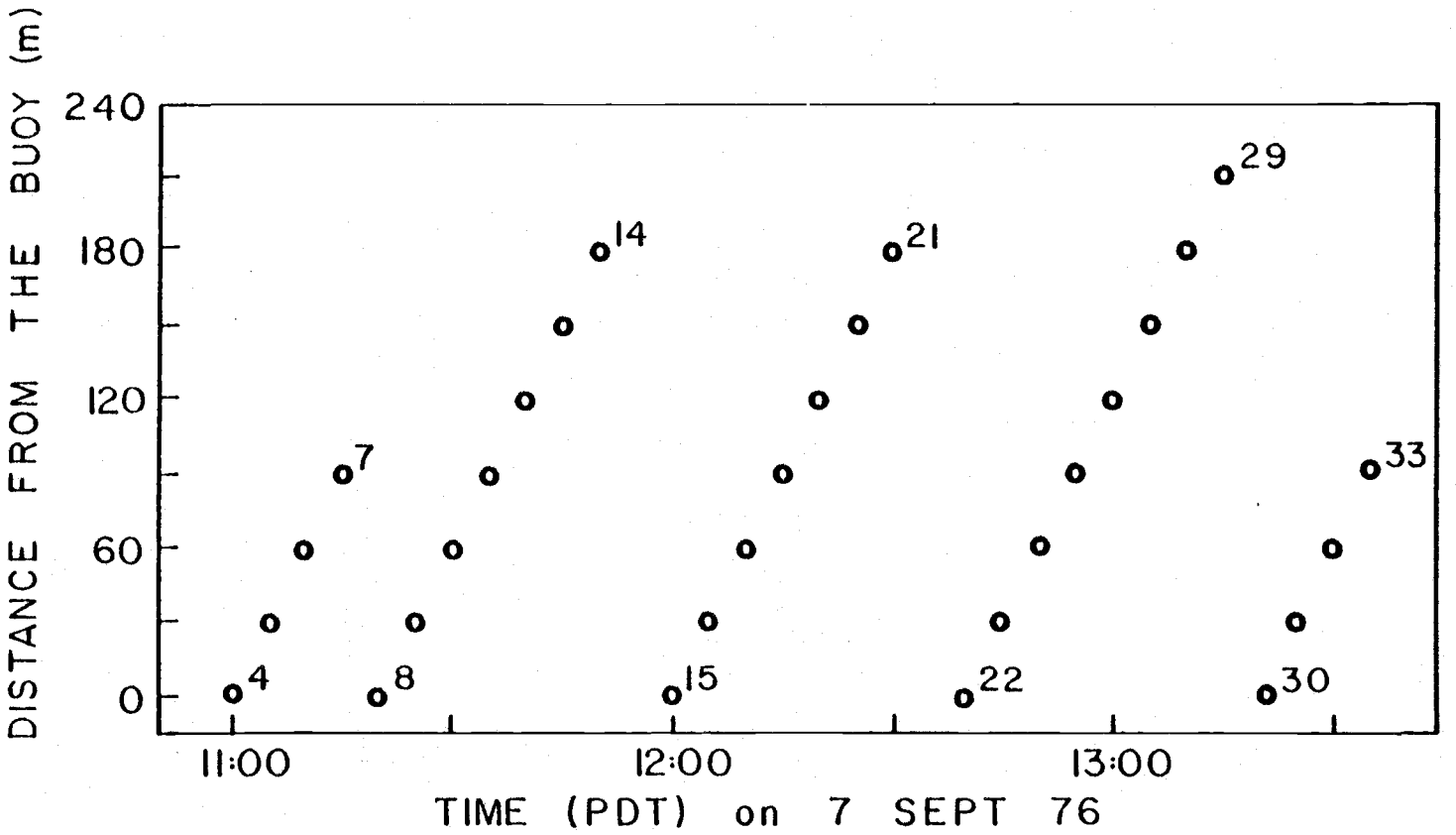

Figure III.5 Sampling station grid for the local ensemble (E-3).

Throughout the local ensemble, this feature, a relatively well-mixed layer at 25 m depth, was identifiable in every profile. Details of its structure varied systematically within each drift sequence and this pattern repeated on each sequence. Along each drift line, with increasing distance from the marker buoy: (1) the layer temperature increased, corresponding to an average horizontal gradient of 1.2×10^{-3} $^{o}C/m$; (2) its upper and lower boundaries became perceptibly sharper; and (3) its thickness increased, roughly from 1 m to 2 m.

These trends are indicated in Figure III.6: in (a), profile segments are offset according to location to depict the two dimensional structure of the layer; in (b), segments from a drift sequence are superimposed to reveal the horizontal temperature gradient; and in (c), segments at the same distance from the buoy, but from three different drifts are superimposed, illustrating the stability of the structure over the sampling period. Only a lower bound for the layer's horizontal extent can be established; on a transect to shore immediately following the midlake sampling, the layer was evident 1.7 km from the marker buoy.

The observed variability of this feature within the sampling grid of Figure III.5 suggests that in the upper thermocline, the current in the sampling (drift) direction was very weak and, in the cross-drift direction, the product of speed and horizontal temperature gradient was small. At least at this level then, advective effects were negligible compared to real horizontal

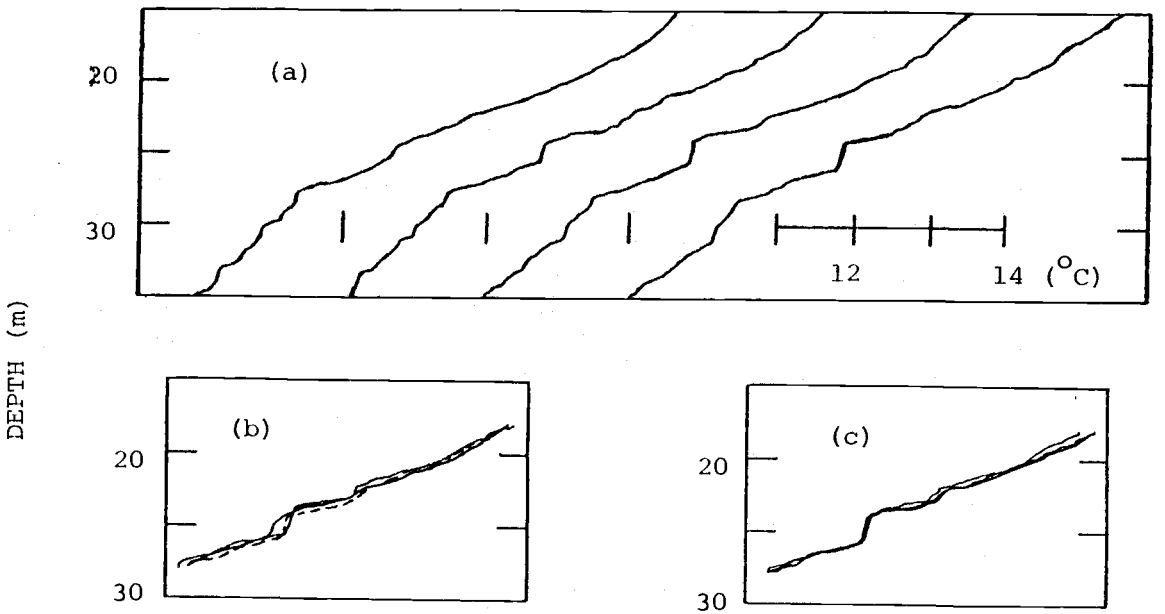

Figure III.6 Horizontal variability of a thin, mixed layer at 25 m depth. (see text for details)

structure referred to the marker buoy's location.

E. Elementary ensemble statistics.

Preceding sections of this chapter have dealt with the formation and qualitative description of three ensembles of temperature profiles, each covering a different range of time and horizontal length scales. To facilitate the characterization and inter-comparison of these sets, we consider now, for each, the depth distribution of ensemble mean temperature and standard deviation shown in Figure III.7. All discussion in the remainder of this chapter will refer to water below the mixed layer unless stated otherwise. Also, hereafter, the ensembles will be referred to as E-1, E-2, and E-3 (see Table III.1).

The mean temperature profiles are substantially the same for all three sets, remarkably so for E-1 and E-2. More structural detail survived the ensemble averaging in E-3, most notably the thin mixed layer at 25 m. Thus, the variability,

$$T_i'(z) = T_i(z) - \overline{T}(z) \qquad \text{(III.E.1)}$$

of a constituent profile $T_i(z)$ about its ensemble's mean profile $\overline{T}(z)$ is subject to an ensemble-dependent filter. To illustrate the effect, consider profiles 4 and 30, members of both E-1 (see 7 September in Figure III.1) and E-3 (Figure III.5). The kink at 25 m is a prominent feature of these profiles and it contributes to the perturbation field of E-1. But in E-3, because of its

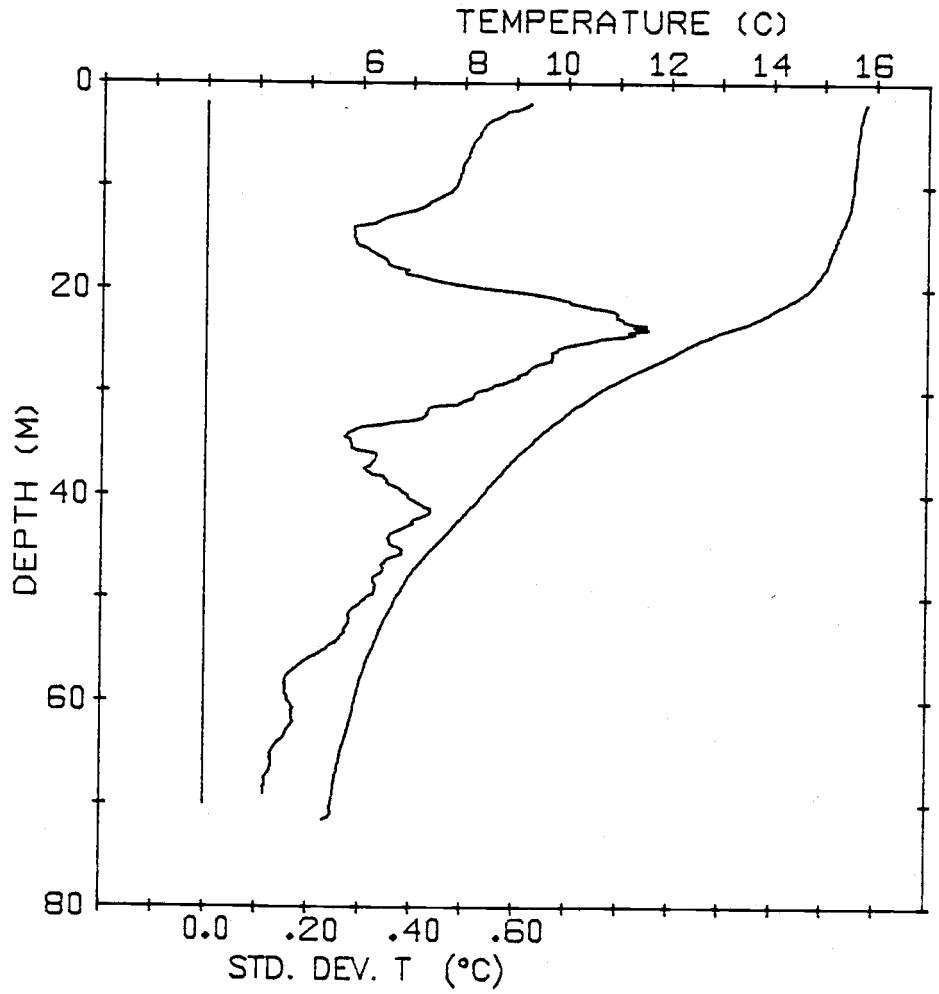

Figure III.7 (a) Ensemble mean and standard deviation temperature profiles for the station ensemble (E-1).

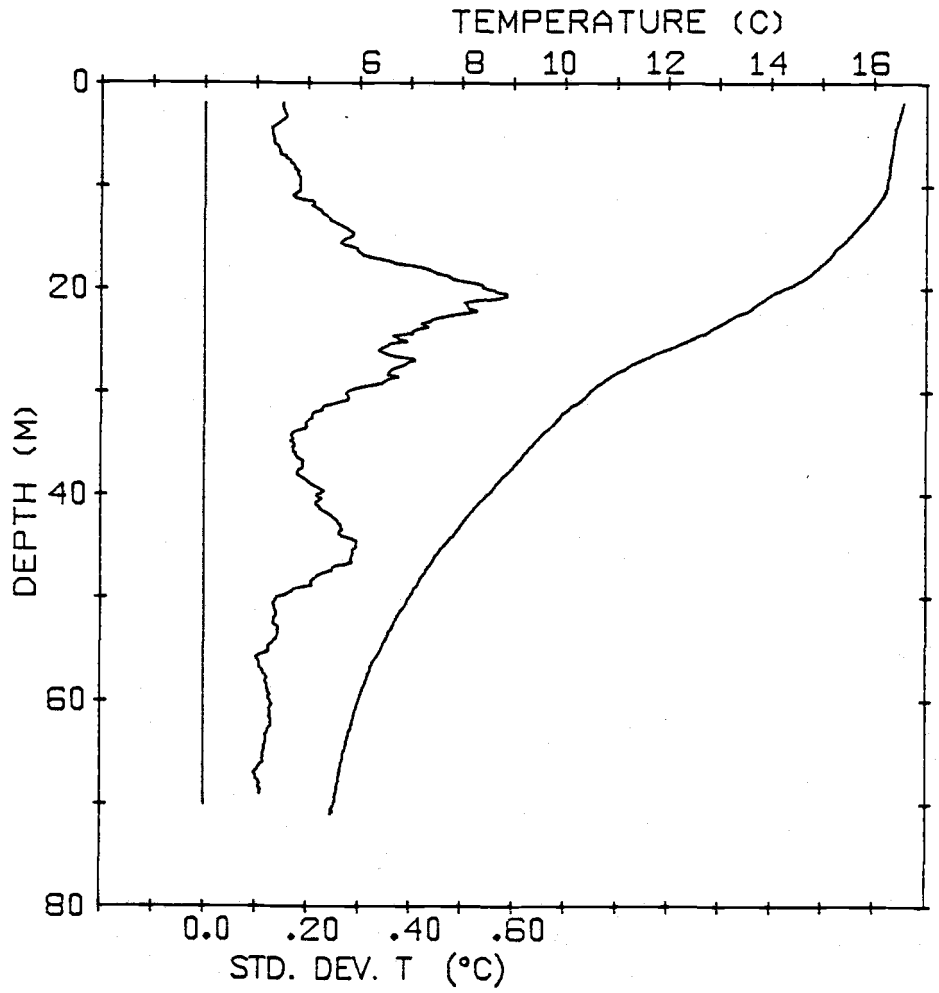

Figure III.7(b) As in (a), but for the transect (E-2).

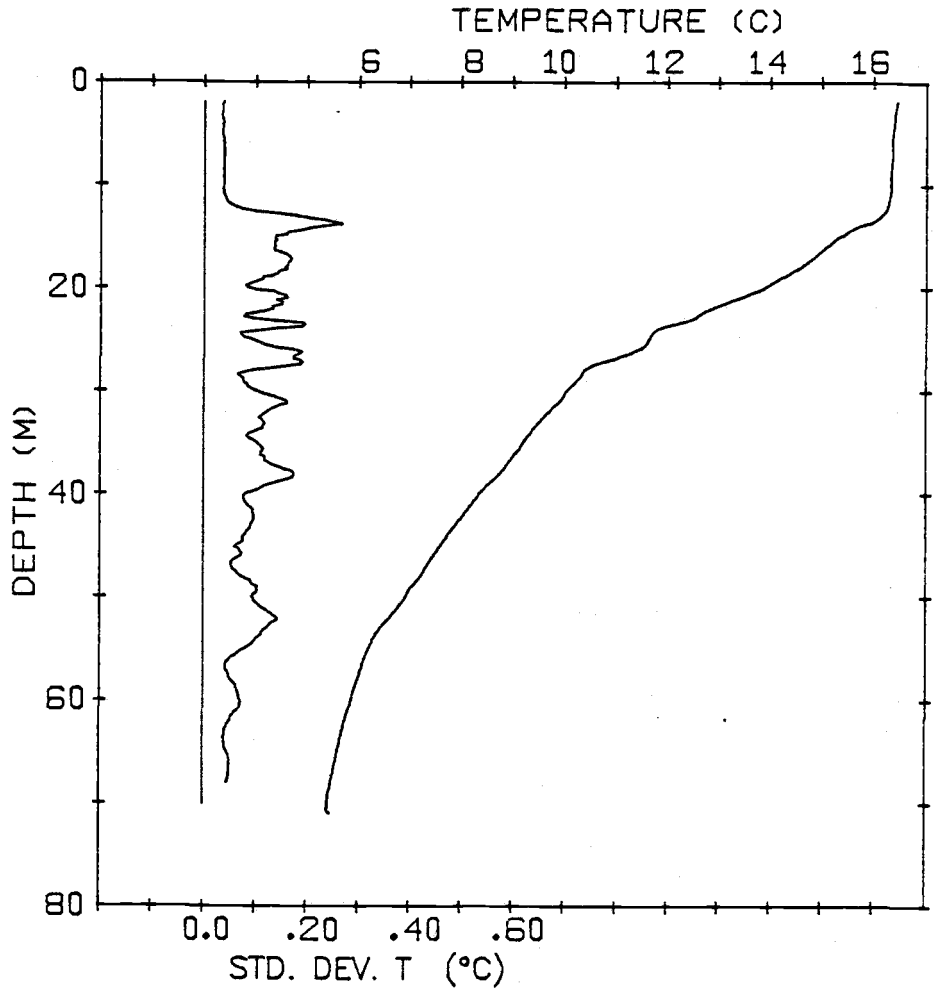

Figure III.7(c) As in (a) but for the local ensemble (E-3)

persistence through the ensemble, and consequent presence in the mean, it will be subtracted out of the $T'(z)$ series. While the potential of this filtering should be appreciated, it must also be observed that the 25 m layer is really the only small-scale feature in the mean profile of E-3.

The standard deviation profiles $s_T(z)$, shown in Figure III.7, are similar in many respects for E-1 and E-2. Not only are the magnitudes roughly comparable, but the vertical shapes have features in common as well, in particular, a local minimum in s_T at about 35 m. There is no corresponding low-gradient interval in the mean profile, so the potential for producing temperature fluctuations was not locally reduced at that depth. The implication, then, is that the responsible physical processes were relatively less active in the vicinity of 35 m.

For the local ensemble, E-3, the $s_T(z)$ profile is quite different from those of the other two sets. Smaller in magnitude at all depths, it exhibits no large-scale vertical structure except a monotonic decrease with depth.

The noise level in s_T is indicated by its value in the mixed layer for E-3, where the real temperature changed very little. Ideal digitization of the raw data introduces noise (Bendat and Piersol, 1971, p. 231) with a standard deviation of $0.29\Delta T$ where ΔT is the least count temperature, about 0.02 ^{o}C. Beyond this are the additional effects of non-ideal curve following with the hand operated cursor and re-zeroing errors in setting up for each profile.

The total noise, approximately a full least count instead of 0.29, is an insignificant component of s_T in E-1 and E-2, and a tolerable level for most of the thermocline in E-3.

The similarity of s_T structure for the station and transect ensembles suggests a dominance in each case by the same generating mechanism. On the other hand, for the local ensemble, limited to (roughly) the horizontal domain of E-1 and the time span of E-2, the large amplitude, large vertical scale variability of s_T is missing. Therefore, it can be associated specifically with the larger time scales of E-1 (greater than 2 1/2 hours) and with the larger horizontal scales of E-2 (greater than 1 km); one or the other is required and there is a sort of horizontal-temporal equivalence.

The buoyancy frequency, N(z) was computed for E-1 and E-3, using $N^2(z) = \alpha g(d\bar{T}/dz)$ with z positive downward and the vertical gradient averaged over 5 m of the mean temperature profile. The N(z) curves are shown in Figure III.8, showing a peak value of about 14 cycles per hour (cph) in the upper thermocline. Use of individual temperature profiles for the vertical gradient, instead of mean profiles, resulted in very similar N(z) curves (not shown).

F. Vertical wavenumber spectra.

For all the temperature fluctuation profiles, T'(z) (formed according to equation III.E.1), vertical wavenumber spectra were computed over various depth intervals in the thermocline. The mean

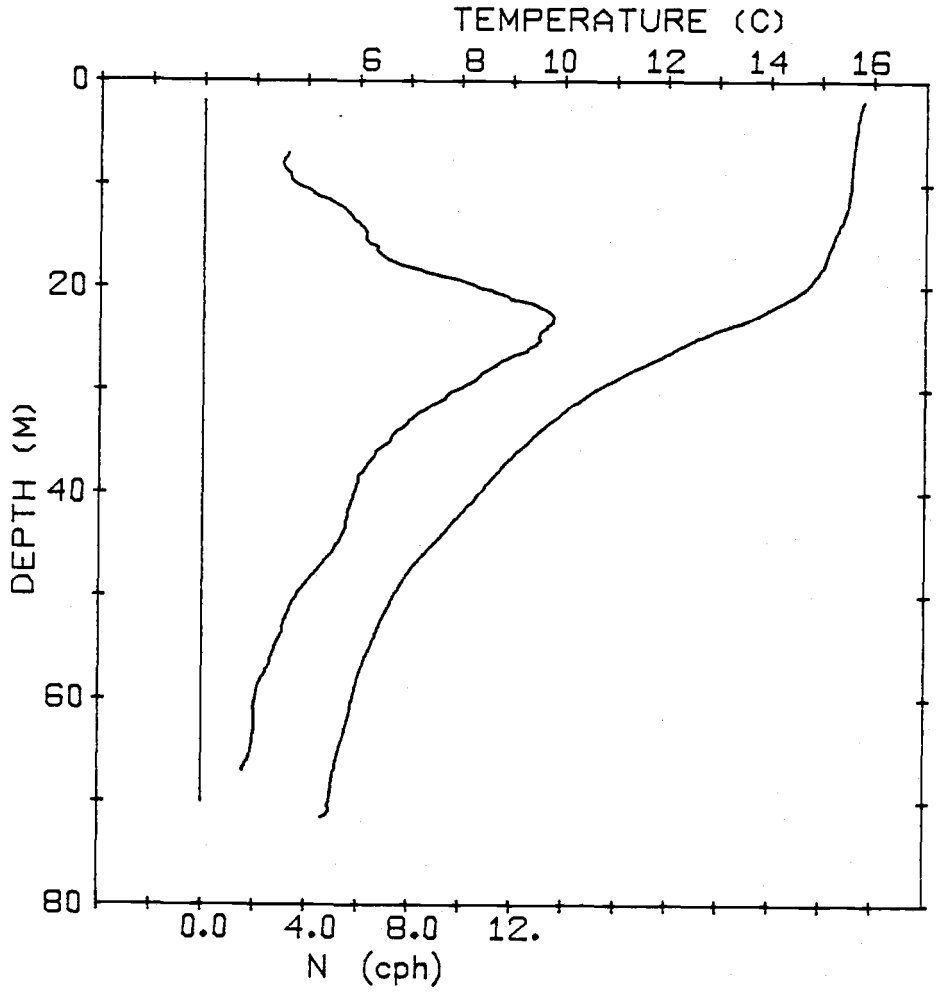

Figure III.8(a) Buoyancy frequency, N(z), for the station ensemble (E-1).

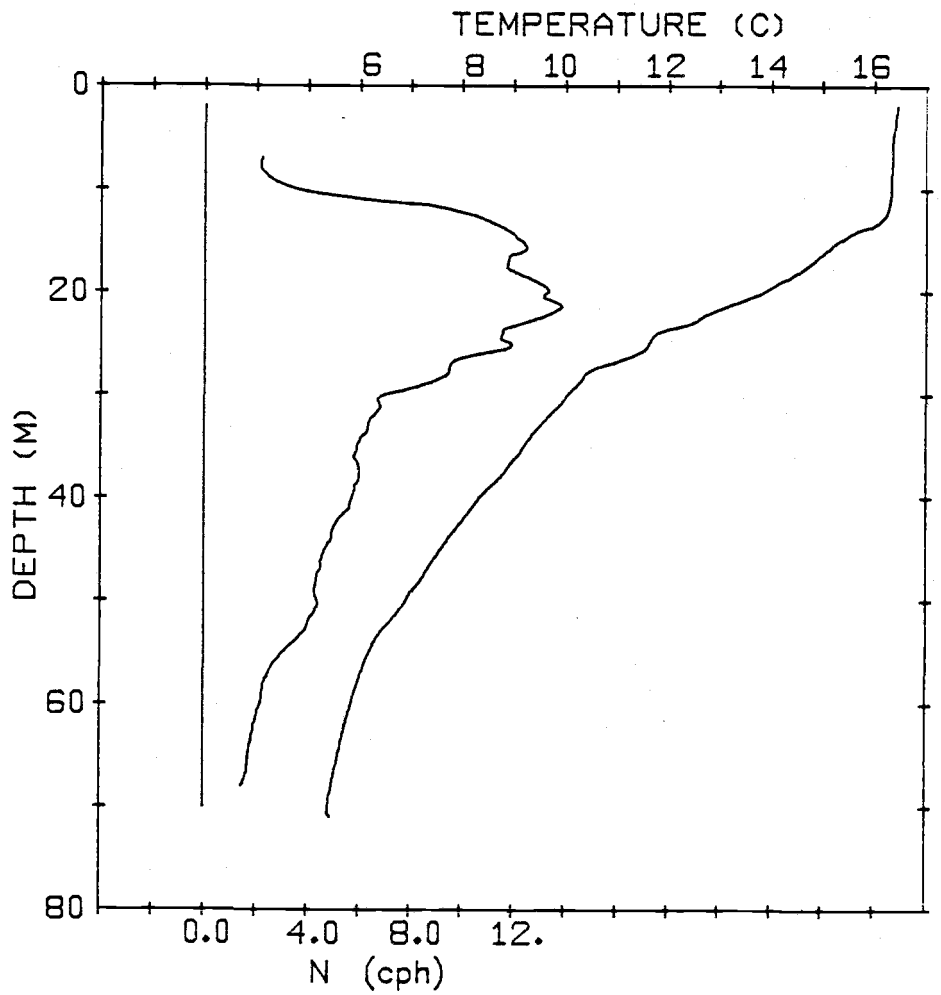

Figure III.8(b) As in (a), but for the local ensemble (E-3)

was removed from each profile segment to be analyzed and then a Hanning data window was applied. Gregg (1977) has discussed the importance of using some window to reduce leakage effects in steeply sloped spectra. The variance reduction due to the window was compensated, and the power spectrum then computed by standard FFT methods (Bendat and Piersol, 1971). Adjacent raw spectral estimates were averaged into wavenumber bands; the number of estimates per band increased as a geometric series, beginning with two at the low wavenumber end, and increasing by 3/2 for each subsequent band (rounded to integers, of course). Band-averaged spectra were then ensemble averaged for each of the three sets: E-1, E-2, and E-3.

Such ensemble spectra, for the depth interval from 15 to 66.1 m, are shown in Figure III.9. Due to the band-averaging scheme, the confidence intervals for the spectral values decrease with wavenumber. They also depend on the number of members in each ensemble (see Table III.1) and in Figure III.9, they apply, except as marked, only to the station ensemble. The variance, $s^2 = (\Delta T)^2/12$, of least count digitization noise may be assumed to be spread over the full wavenumber bandwidth, $(2\Delta z)^{-1}$, (Otnes and Enochson, 1972), contributing $s^2 2\Delta z = \Delta z(\Delta T)^2/6$ to the spectrum. With $\Delta z = 0.1$ m and the temperature least count of $\Delta T = 0.02\ ^{o}C$, this level is $6.7 \times 10^{-6}\ ^{o}C^2$/cpm. Due to the other uncertainties noted before, this must be considered as a lower bound, and the flattening of

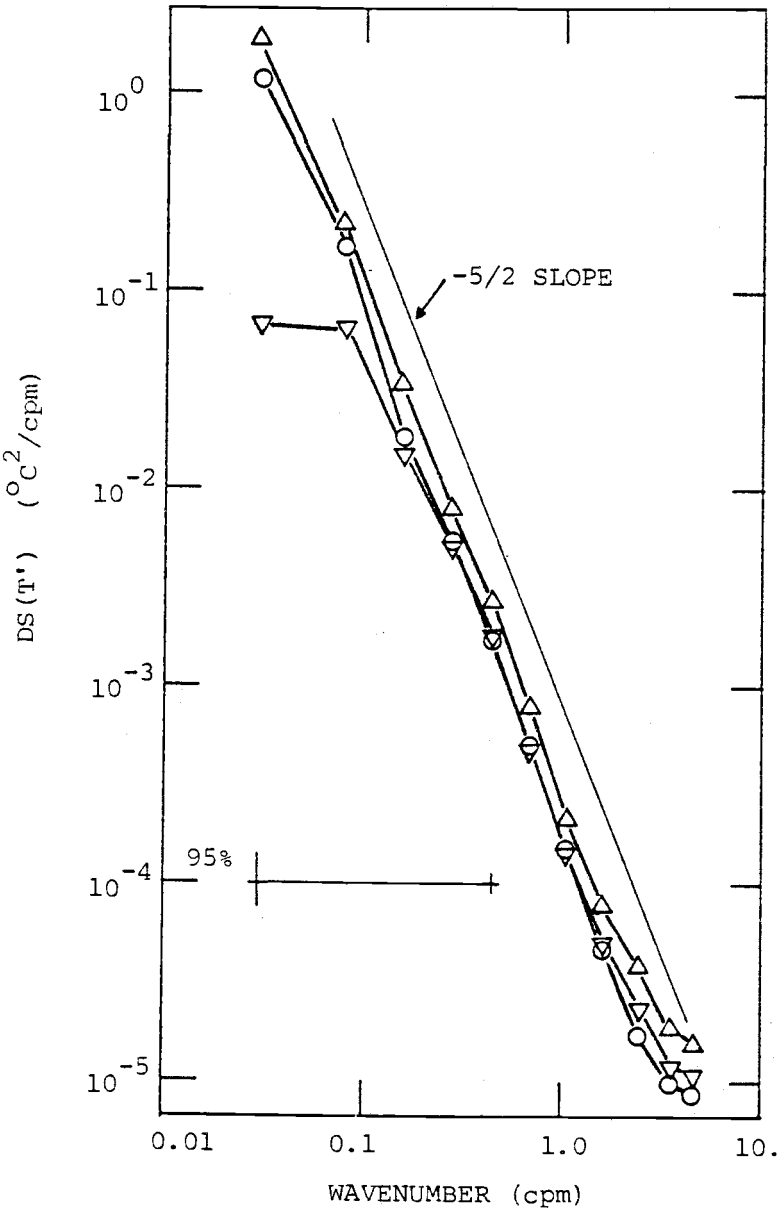

Figure III.9 Vertical wavenumber spectra of temperature fluctuations for all three ensembles over the depth range 15 to 66.1 m. Symbols: △ for Station, E-1; ○ for Transect, E-2; ▽ for Local, E-3.

all the spectra at the highest wavenumbers is thought to reflect the noise level.

Figure III.9 makes it clear that the larger temperature variance of E-1 and E-2 compared to that of E-3 (Figure III.7) was concentrated entirely at low wavenumbers. (Note that the large vertical scales in the standard deviation plots do not, in themselves, reveal typical vertical scales of the temperature perturbations; the ensemble spectra yield essentially different information than would be obtained by computing a spectrum of the standard deviation profiles.) At higher wavenumbers, the spectra are very similar for all three ensembles, strikingly so for E-2 and E-3.

In general, the spectra are nearly linear in this log-log presentation, suggesting a power dependence on wavenumber of about -5/2. Similar results have been reported for oceanic temperature fluctuation spectra in the North Atlantic by Hayes et al. (1975), who analyzed 50 m segments of CTD (conductivity, temperature, depth) profiles at five different depths. Gregg (1977) presented spectra from the main thermocline of the North and South Pacific and the North Atlantic, computed over several hundred meters, and found a low-wavenumber slope of -2, a slope break at 0.06 to 0.1 cpm, and a high-wavenumber slope of about -3.

Over the measured portion of the Lake Tahoe thermocline, the buoyancy frequency varied by a factor of six or seven. To see if the spectral characteristics depended strongly on the local N, or on depth in general, four intervals, centered at 25, 35, 45,

and 54 m were selected for separate analysis. The mean temperature gradient and buoyancy frequency for each interval are shown in Table III.3. Records of 256 points (25.6 m) were used so there was considerable overlap for adjacent intervals. However, the Hanning window attenuates the ends of each series and it is the central part that dominates the spectrum. Results for E-1 and E-3 are shown in Figure III.10.

For E-1, the spectra separated fairly uniformly to either side of the spectrum of the 15-66.1 m interval, retaining the linear shape and approximate slope. Similar results were reported by Hayes et al. (1975) over a much greater range of depths at their Atlantic site; there, the buoyancy frequency varied from about 0.5 to 2.5 cph. For E-3, the depth effects were not as uniform in wavenumber. Part of the low wavenumber behavior may be attributed to the filter effect the E-3 sampling has on these scales. Also, despite the presence of the 25 m kink in the ensemble mean of E-3 (Figure III.7(c)), the details of its structure did vary through E-3 and must have contributed something to the T' field. This may account for some of the qualitative differences of the high wavenumber portion of the 25 m spectrum (somewhat flatter slope and relatively higher level).

G. Horizontal-temporal coherence in the local ensemble.

In previous sections of this chapter, different methods have been used to describe and characterize the variability or structure

TABLE III.3. Mean gradient and buoyancy frequency for the short-interval spectra shown in Figure III.10.

Mid-depth (m)	Ensemble E-1 dT/dz -(°C/m)	Ensemble E-1 N -(cph)	Ensemble E-3 dT/dz -(°C/m)	Ensemble E-3 N -(cph)
25	0.407	12.4	0.382	11.5
35	0.226	7.4	0.170	6.2
45	0.166	5.1	0.142	4.8
54	0.080	2.8	0.107	3.3

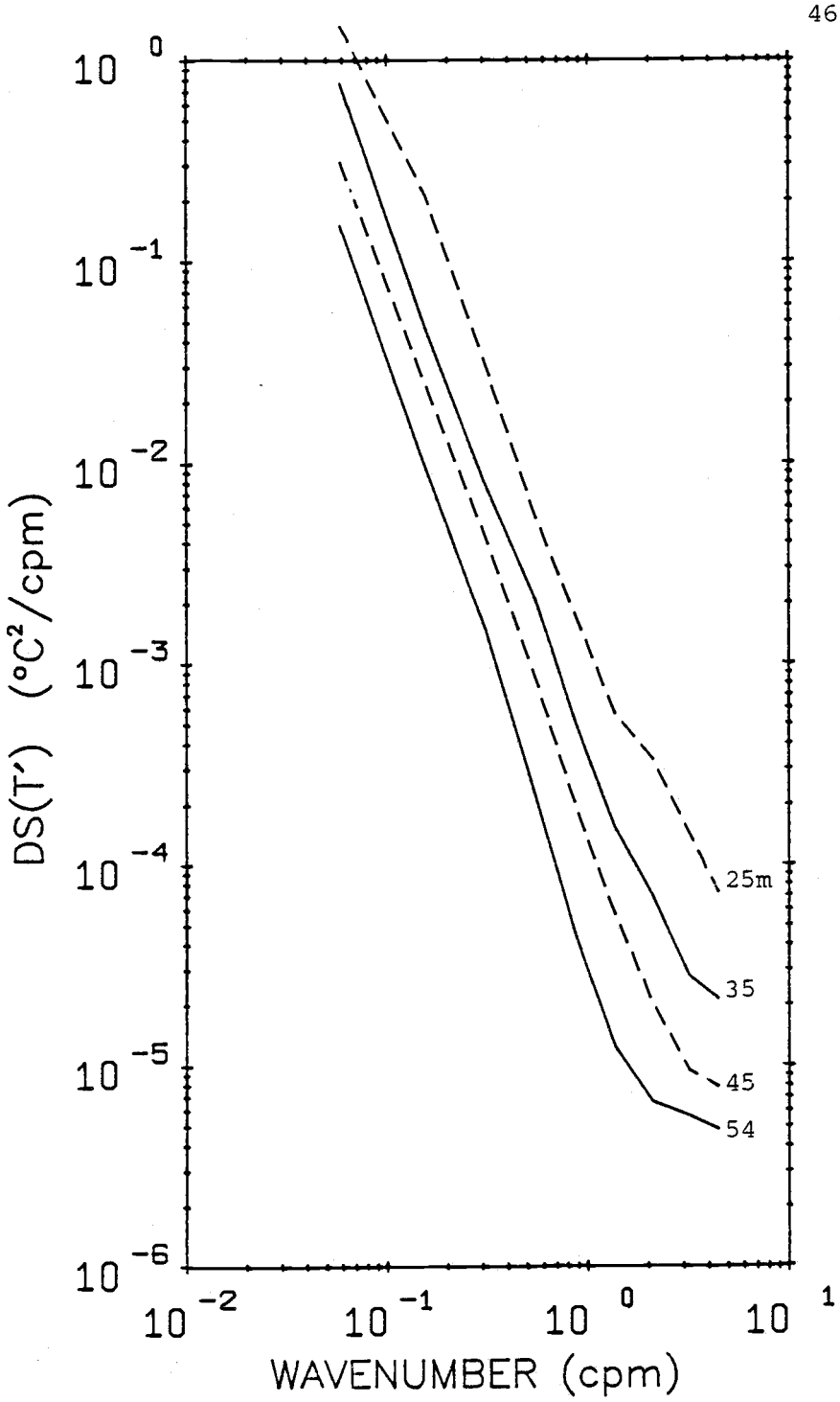

Figure III.10(a) Short interval temperature spectra at four depths for the station ensemble (E-1). DS denotes dropped spectrum.

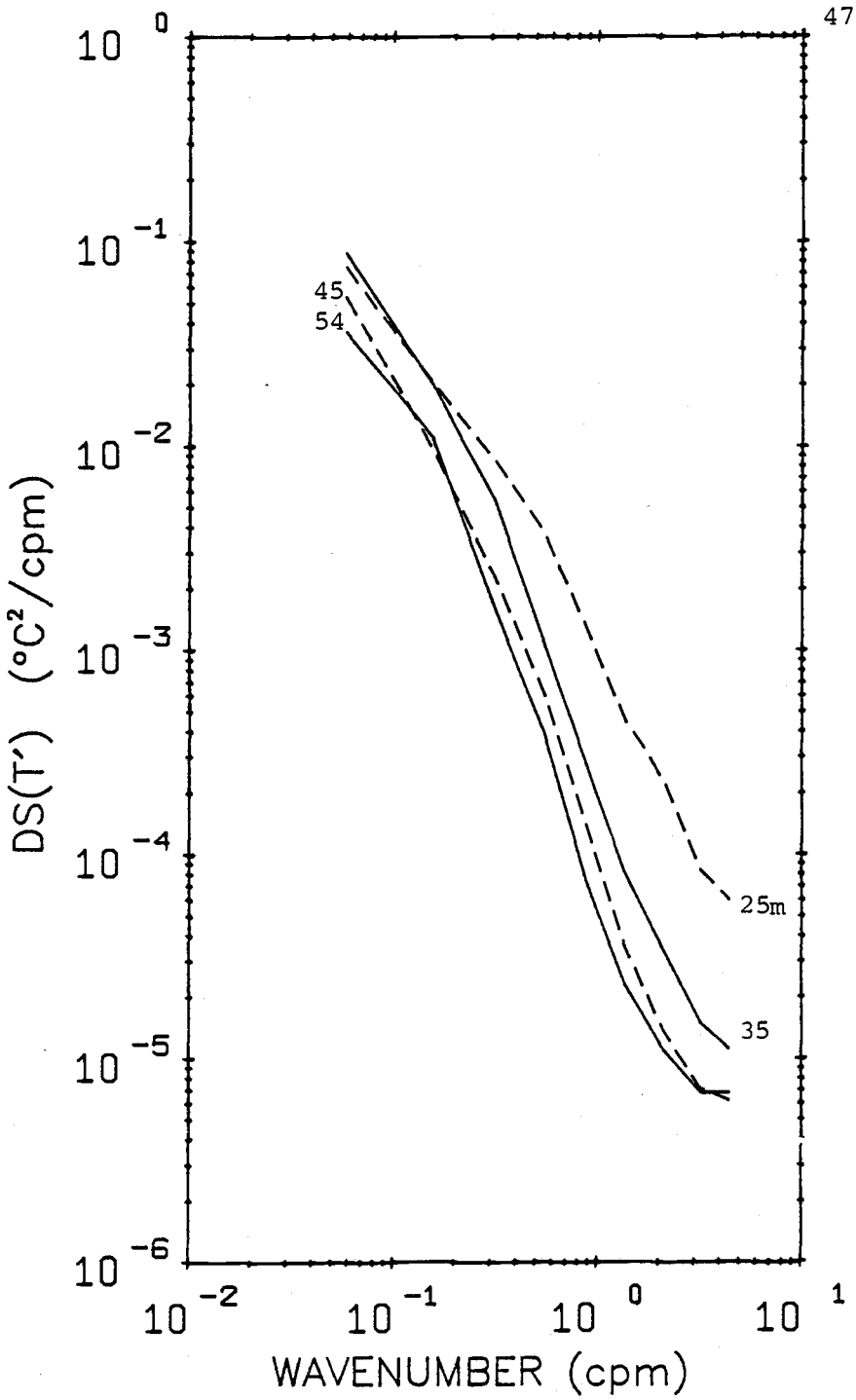

Figure III.10(b) As in (a), but for the local ensemble (E-3).

of each ensemble; these characteristics have been compared and contrasted from one ensemble to another. The sampling pattern for the local set (Figure III.5) invites a closer examination of the variability within the ensemble. Two approaches follow.

1. Cross spectral analysis. Using the same windowing and band-averaging procedures applied to the spectra in section F, cross spectra were computed for various pairs of profiles in the local ensemble over the 15-66.1 m depth interval. To minimize the effects of position uncertainty, both members of a pair were always selected from the same drift line. However, stationarity was assumed, so that results for pairs with equal separation could be grouped, thus improving the statistical definition. For example, all of the following pairs of profiles (see Figure III.5) represent a separation of 150 m and 25 minutes: (8,13), (9,14), (15,20), (16,21), (22,27), (23,28), and (24,29). Table III.4 summarizes the pair grouping.

Band-averaged auto and cross spectra for each pair were ensemble averaged over the pair group before computing coherence and phase. Results as a function of vertical wavenumber, with separation as a curve parameter, are shown in Figure III.11. Due to band averaging and unequal group sizes, the number of degrees of freedom is different for each point. Coherence points below the 95% significance level are approached by dashed line segments, as are the phases corresponding to those coherences. For the smallest separation, 30 m and 5 minutes, the coherence is significant for wavenumbers up to about 0.45 cpm. For greater separations

TABLE III.4. Pair groups drawn from the local ensemble (E-3), used in cross-spectral analysis.

Separation		Number of pairs
Horizontal (m)	Time (min)	
30	5	25
60	10	20
90	15	15
120	20	10
150	25	7
180	30	4

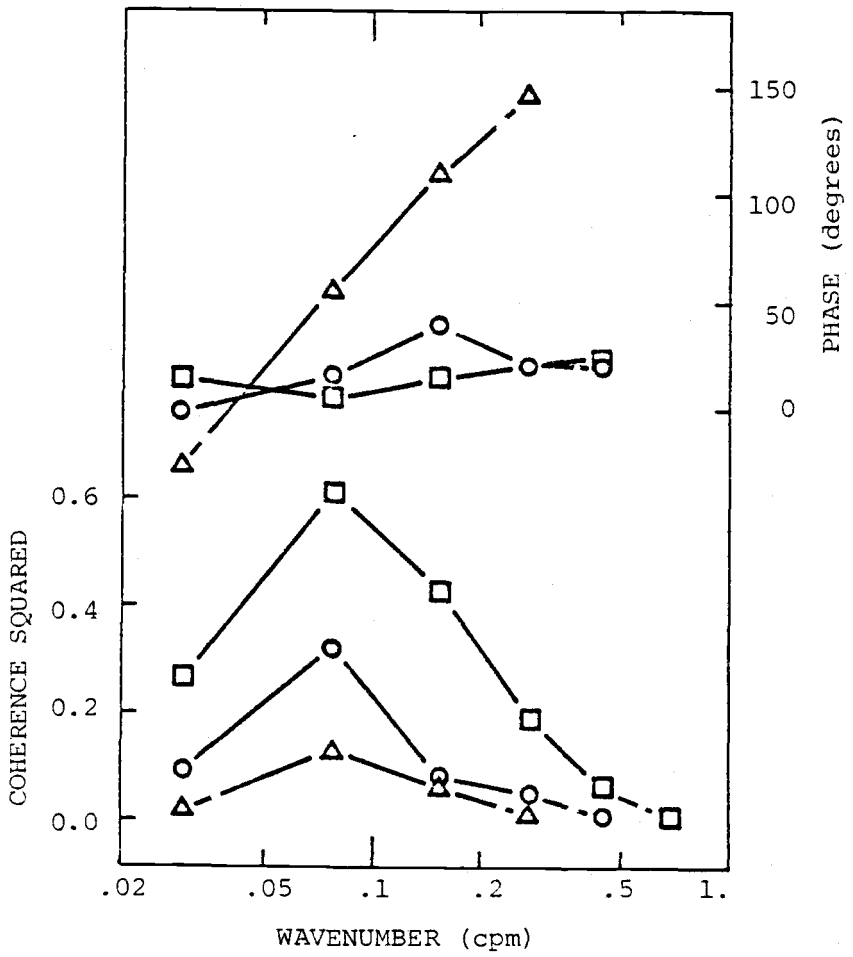

Figure III.11 Coherence and phase spectra, with pair separation as a curve parameter. Separations: □ 30 m, 5 minutes; ○ 60 m, 10 minutes; △ 90 m, 15 minutes. Coherence points not significant at 95% level are approached by a dashed segment as are the corresponding phase points.

the coherence is lower at all wavenumbers and becomes insignificant at smaller wavenumbers.

The coherence does not fall monotonically with increasing wavenumber. A similar result was found by Stegen et al. (1975) in the upper thermocline of the tropical North Atlantic. In the Lake Tahoe data, the relatively low coherence at the lowest wavenumber band may be attributed, at least in part to the attenuation of these scales by the sampling (filter) effect of the local ensemble. At any rate, the greatest coherence occurs near 0.1 cpm, so the coherence and phase for the two nearest wavenumber bands were plotted for all separations and this is shown in Figure III.12. All coherence points there are significant at the 95% level.

The coherence decreases rapidly with increasing separation and is smaller at all separations for the smaller vertical scales. We may use coherence = 0.5 (coherence squared = 0.25) to define decoherency scales of separation. For the 13 m wavelength this occurred at 70 m and 12 minutes; for the 6.5 m wavelength the scales were 44 m and 7 minutes. In a study of dropped lagged coherence in the North Atlantic, Hayes (1975) reported that features with vertical wavelengths smaller than 10 m had lost coherence in his shortest lag time, 12 minutes, which is consistent with the present findings.

After the coherence bottoms out at about 90 m and 15 minutes, it begins to rise slowly with separation. It should be noted that there are fewer degrees of freedom at larger separations,

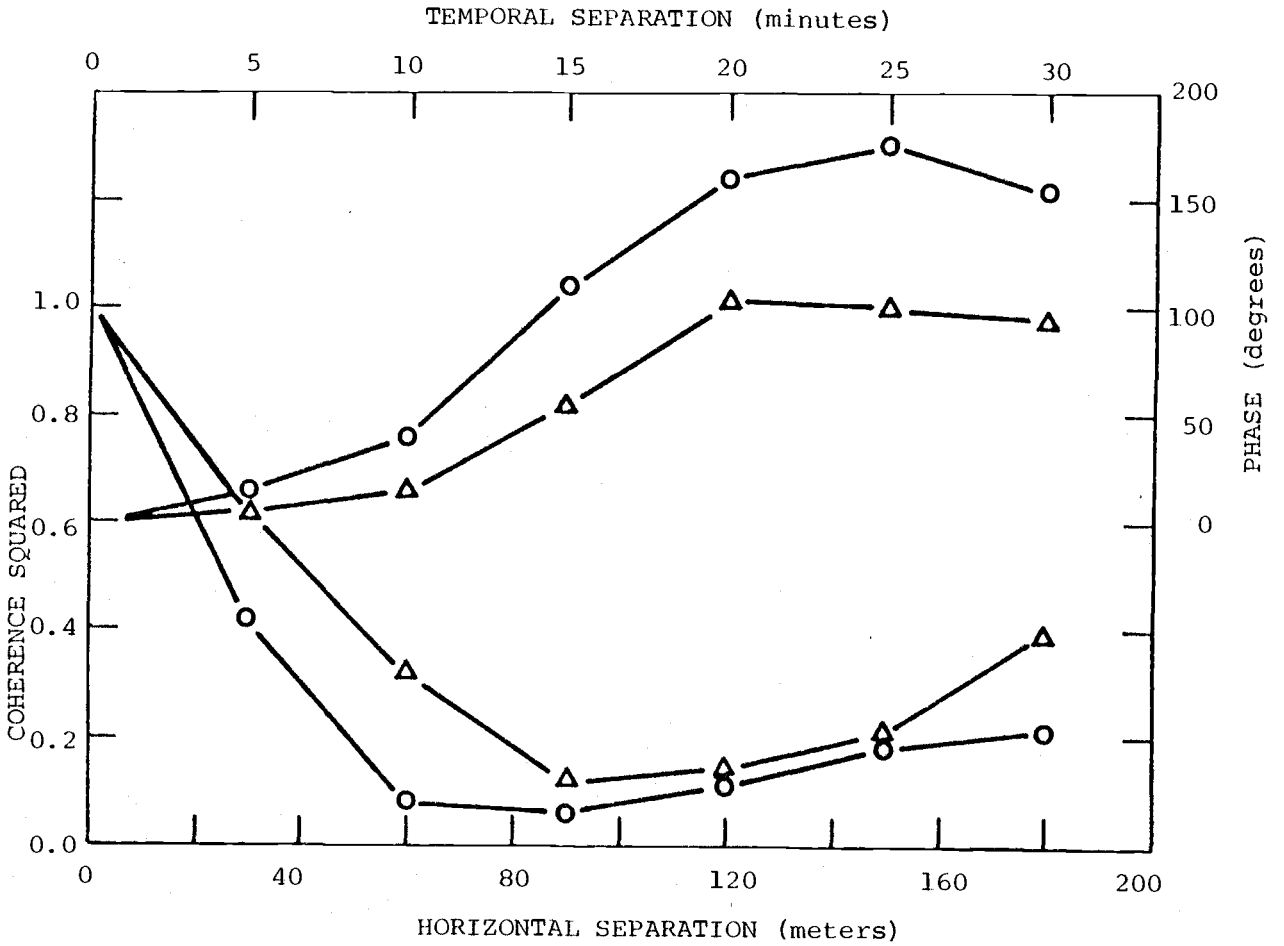

Figure III.12 Coherence and phase, plotted against separation, for two values of the vertical wavenumber. Symbols: Δ 0.0781 cpm (13 m wavelength); O 0.156 cpm (6.5 m wavelength).

corresponding to the reduced number of pairs (Table III.4); nevertheless the coherence appears to be significant. Further, it is common in spectral analysis to find the phase become very erratic when the coherence is truly lost. But the phase in Figure III.12 shows a fairly well behaved rise with increasing separation.

Cross spectra were also computed for pairs of adjacent profiles in the transect ensemble. Only in the lowest wavenumber band, 0.029 cpm, was the coherence significant, with a value of 0.7 and a phase angle of -19 degrees. The average pair separation was 880 m and 11 minutes. This result may not be interpreted as a straightforward extension of the coherence data of the local ensemble because it deals with the vertical scales not well represented in the latter.

2. Variability about a smoother mean profile. We have discussed in section III.E how use of the ensemble mean profile in forming fluctuation profiles according to (III.E.1) results in the removal of slow or persistent features from the perturbation field. In this section, a different approach to the formation of $T_i'(z)$ series is adopted. We use

$$T_i'(z) = T_i(z) - P_i(z) \qquad \text{(III.G.1)}$$

where $P_i(z)$ is a polynomial, fit to $T_i(z)$ by least squares methods. A low order polynomial will follow the general trend of $T_i(z)$,

but will not contain finestructure features. After some experimentation, cubic polynomials were judged appropriate.

The most obvious persistent feature of this set is the thin mixed layer at 25 m discussed in section III.D, so a depth interval of 15-40.5 m was chosen for analysis. Correlation coefficients were computed for various pairs of $T_i'(z)$ series according to

$$R_{ij} = (s_i s_j n)^{-1} \sum_{k=1}^{n} (T_i'(z_k) - \overline{T_i'})(T_j'(z_k) - \overline{T_j'})$$

where $\overline{T_i'}$ and s_i are the series (not ensemble) mean and standard deviation of the i-th fluctuation series. Again, stationarity of this statistic was assumed, i.e., that R_{ij} depended on separation, but not on absolute location of the i-th and j-th profiles. Correlations for pairs with equal separations were averaged.

The selection rules were relaxed a bit from those used with the cross spectra, but still, the horizontal distance between two profiles was regarded as known only if: 1) both stations were on the same drift line, or 2) one of the stations was at the marker buoy.

Figure III.13 shows correlation values as a function of horizontal and temporal separation. For pairs where both members were drawn from the same drift line, the results fall on the dashed line. At the longer time separations, only one pair could be formed. Such single-pair correlations were combined with their nearest (single-pair) neighbor on the map, and the average written with an overbar.

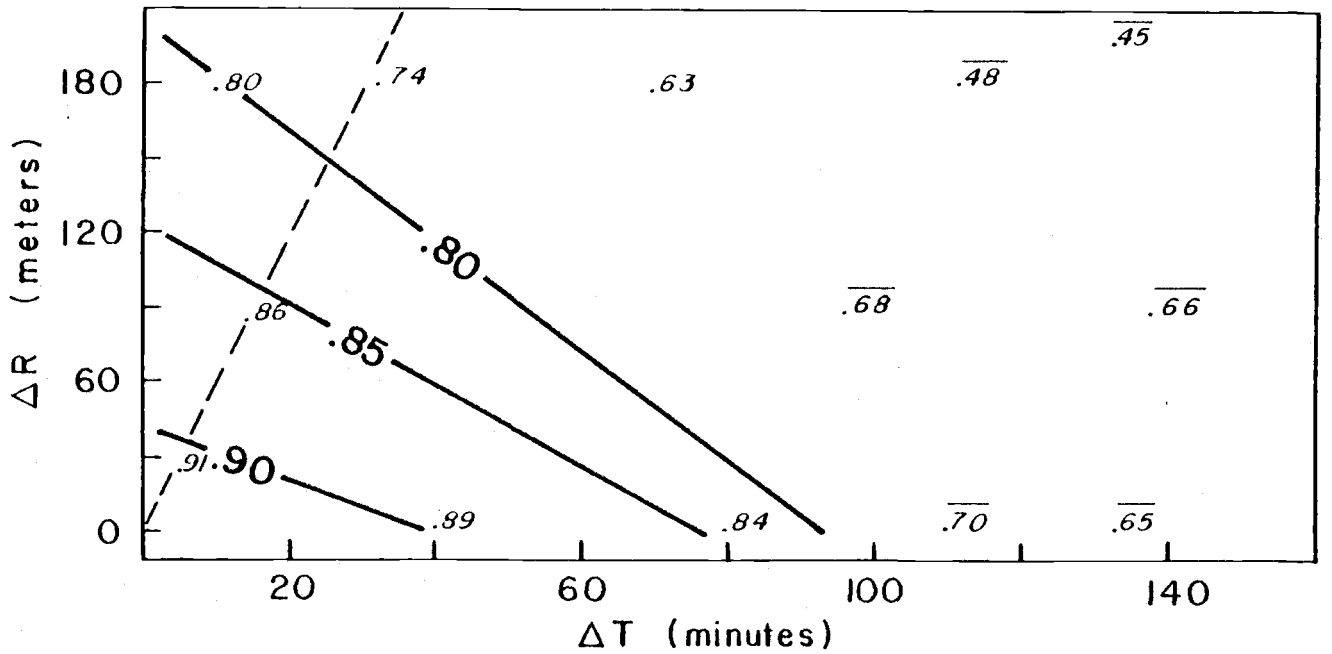

Figure III.13 Correlation map for variability about a polynomial trend over the depth range 15 to 40.5 m. Values on the dashed line are for station pairs where both members were drawn from the same drift line.

If the variability were wholly temporal, lines of constant correlation would be perpendicular to the time separation axis. On the other hand, a "frozen" field of horizontally varying structure would be represented by correlation lines parallel to the time axis. The rough contours drawn in Figure III.13 indicate that both components of variability were important.

H. Summary.

From the finestructure data (observations with the TD instrument) the following characteristics of temperature variability in the Tahoe thermocline were found.

There was a well-defined equilibrium state which persisted throughout the measurement period. On seasonal scales, the lake had not yet begun the process of autumn cooling and intense mixing.

About this equilibrium, variability on many space-time scales was observed. Formation of ensembles of profiles permitted some isolation of horizontal and temporal scales. Over time scales of days to weeks, or over horizontal scales of several km, relatively large amplitude temperature fluctuations were observed. Near 35 m depth, profiles of ensemble standard deviation temperature exhibited a local minimum, suggesting less activity there in the underlying physical processes.

In contrast, for sampling limited to 2 1/2 hours and to about 200 m horizontally, the ensemble variability was of smaller magnitude. Further, no features in its vertical structure gave particular significance to any one depth interval.

Vertical wavenumber spectra of temperature fluctuations fell steeply, roughly as the -5/2 power of the wavenumber. Among the three ensembles, the principal distinction was at the lowest wavenumbers, where the spectral level of the local set (small horizontal-temporal scales) was much lower than that of the other two sets.

At the higher wavenumbers, the spectra of all three sets were similar, indicating a stationarity in the processes that dominate the variance of small vertical scales.

Cross-spectral computations with the local set revealed a coherence that was highest for wavenumbers of order 0.1 cpm. At these vertical scales, the coherence dropped to 0.5 (coherence squared = 0.25) at horizontal-temporal separations of roughly 50 m and 10 minutes.

These results on scales of variability represent only a first step toward development of a full frequency-wavenumber spectrum for the temperature field, but should provide some perspective and organizational structure for future work. Similarities of some features of the Tahoe spectra (and cross spectra) to oceanic results support the idea that similar dynamics control the small-scale structure in both environments. Thus, Tahoe could find extensive use as a "laboratory" for studying some oceanic phenomena. In the next chapter, where internal wave concepts are applied to the present results, the correspondence with oceanic spectra becomes striking.

CHAPTER IV. INTERPRETATION AND DISCUSSION OF THE FINESTRUCTURE RESULTS

A likely physical source for the observed fine-scale temperature variability is the transient distortion of the mean temperature field by internal wave motion. Alternatively, the observed structures might represent persistent features of some mixing events which could themselves very well be associated with unstable internal waves, or, perhaps, with non-wavelike interleaving processes.

In this chapter, the internal wave connection is pursued. The salient results of Chapter III are found to be consistent with the hypothesis that internal wave displacements, wrinkling an otherwise smooth temperature distribution, produced the variability in the finestructure of the thermocline.

We begin by developing some relevant concepts from internal wave theory. These are first applied to the ensemble standard deviation temperature profiles and then to the spectral results.

A. Vertical structure of internal waves.

The linearized equations of motion for a rotating, inviscid, Boussinesq fluid can be combined into one equation for w, the vertical velocity (Phillips, 1977)

$$\nabla^2 w_{tt} + N^2(z)\nabla_h^2 w + f^2 w_{zz} = 0 \qquad \text{(IV.A.1)}$$

where the subscripts denote differentiation with respect to time, t, and depth, z, ∇^2 is the full Laplacian operator, ∇_h^2 is the horizontal Laplacian, N is the buoyancy frequency, and f is the Coriolis parameter. The latter are defined by $N^2 = (g/\rho_0)\,\bar{\rho}_z$ where g is the acceleration of gravity, ρ_0 is a constant reference density, and $\bar{\rho} = \bar{\rho}(z)$ is the mean density profile; and by $f = 2\Omega\sin(\text{latitude})$ where Ω is the angular velocity of the rotation of the earth.

We now assume the flow variables have the form of horizontally propagating waves, with the vertical behavior contained in "wavefunctions." Taking x in the propagation direction, we can write, for example,

$$\begin{bmatrix} u(x,z,t) \\ w(x,z,t) \\ \zeta(x,z,t) \end{bmatrix} = \begin{bmatrix} U(z) \\ W(z) \\ Z(z) \end{bmatrix} \exp\,(i(kx - \omega t)) \qquad \text{(IV.A.2)}$$

where u is the horizontal velocity, ζ is the vertical displacement, k is the horizontal wavenumber, and ω is the frequency. Using this w in (IV.A.1) yields an equation for the vertical velocity wavefunction

$$W_{zz}(z) + m^2(z)W(z) = 0 \qquad \text{(IV.A.3)}$$

$$m^2(z) = k^2 \frac{N^2(z) - \omega^2}{\omega^2 - f^2} \qquad \text{(IV.A.4)}$$

The wavefunctions are related. Since $w = \zeta_t$, we have $W = -i\omega Z$, and substituting this in (IV.A.3), we find that Z and W satisfy the same equation, i.e.

$$Z_{zz}(z) + m^2(z)Z(z) = 0 \qquad \text{(IV.A.5)}$$

Through the continuity equation, $u_x = -w_z$, we get

$$U(z) = (i/k)W_z(z) = (\omega/k)Z_z(z) \qquad \text{(IV.A.6)}$$

Since it is the vertical displacement that is most readily related to temperature fluctuations, we will devote the remainder of this section to consideration of (IV.A.5).

1. m(z) approximately constant. The difficulty with (IV.A.5) lies in the variability of m(z), which reflects the character of the stratification through (IV.A.4). There may be circumstances in which m varies little over the vertical scale of motion of the internal waves. Then, taking m as locally constant, (IV.A.5) has solutions of the form

$$Z(z) = A \exp(imz) \qquad \text{(IV.A.7)}$$

with A an arbitrary constant. Thus mz may be added to the phase in (IV.A.2), m being the local vertical wavenumber component. This

solution provides a basis for comparing some features of independent waves at different depths but doesn't describe the continuous changes in waves which extend over a depth range in which the variation of m must be taken into account.

2. m(z) slowly varying. A very useful asymptotic solution to (IV.A.5) is applicable if the local vertical scale of the waves, m^{-1}, is small compared to the vertical scale of N(z) (and hence m(z)). This is the "WKB" approximation, (Nayfeh, 1973) which, for $m^2(z)>0$, has the form

$$Z(z) = Am^{-1/2}(z)\exp(i\int^z m(z')dz') \qquad \text{(IV.A.8)}$$

where, again, A is an arbitrary constant. With N(z) no longer held constant, there is the possibility of $m^2(z)$ being positive in some depth intervals and negative in others. The depths at which m^2 goes through zero, known as "turning points," occur where N(z) is equal to the wave frequency. Although (IV.A.8) is valid only well away from turning points, Eriksen (1978) has, with similar asymptotic methods, analyzed waves trapped between two turning points and developed solutions that are uniformly valid, even across the turning depths.

The importance of (IV.A.8) to the present work lies in the depth dependence it expresses for the displacement wavefunction. First, it is oscillatory in z and Kundu (1976) has shown that m(z) may still be interpreted as the local vertical wavenumber. But

the oscillation is modulated by a depth-dependent coefficient so that, as waves propagate into a region of weaker stratification (smaller N, smaller m), their vertical wavenumber decreases as m(z) and the amplitude factor for their displacement increases as $m^{-1/2}(z)$. Through (IV.A.6), the amplitude factors for horizontal and vertical velocities scale with $m^{1/2}(z)$ and $m^{-1/2}(z)$ respectively. Further, if $\omega^2 << N^2$, then (IV.A.4) shows that, although m still depends on ω, the depth dependence of m and N become simply proportional. Thus, N can replace m in all the depth scaling mentioned in this paragraph, and the scaling is then independent of frequency.

These WKB ideas have sometimes been applied with success in internal wave studies, even when the vertical wave scale was not small compared to the length scale of N(z), (Kundu, 1976, Mied and Dugan, 1974).

3. Vertical modes. Regardless of the variability of m(z), there may be physical boundaries at certain z values, for example the basin floor and the air-water interface. Waves with a vertical wavelength comparable to the domain between boundaries, and waves (of any wavelength) capable of propagating over that domain without significant dissipation, will develop a modal structure with a set of wavefunctions and corresponding horizontal wavenumbers for any given frequency.

For constant N (and m), modes of Z will be just like standing waves on a vibrating string, fixed at both ends. For variable

N (and m) the boundaries may be real or they may be turning points. Analytical modal solutions are possible if N is slowly varying (Eriksen, 1978); otherwise, numerical techniques are required.

B. Application to the standard deviation profiles.

Although the preceding section has presented some general concepts from internal wave theory that bear on the vertical distribution of displacements, further information is required to relate these ideas to a specific situation. Part of this information is environmental: the local Coriolis parameter, the basin depth, the measured N(z) profile. But even within these constraints, enormous variety is allowed the internal wave field depending on frequency content, modal content, etc.

Consider the data. If the observed temperature fluctuations, T', were produced by internal wave vertical displacements, ζ, the two are related by

$$T'(z) = \zeta(z)(d\bar{T}/dz) \qquad \text{(IV.B.1)}$$

where $\bar{T}$ is the ensemble mean temperature. Thus, the standard deviation temperature data, s_T, shown in Figure III.7 can be converted to standard deviation displacements, s_ζ, by dividing by the local gradient since, of course, $s_T = s_{T'}$. The internal wave displacement interpretation applies only in the thermocline; temperature fluctuations in the epilimnion and the transition

layer below it reflect, instead, non-wavelike mixed layer processes such as turbulent eddy motion and entrainment.

Distributions of $s_\zeta(z)$, where a 5 m average was used for the temperature derivative, are shown in Figure IV.1 for E-1 and E-3. The gradient scaling has changed the shape of s_ζ compared to s_T, but the two ensembles are still distinct in the same way. Larger amplitude displacements dominate E-1 and there is large scale vertical structure associated with their generation; in particular, there is less activity around 35 m depth. Displacements in E-3 are smaller and show a general trend of increasing amplitude with depth. Evidently, rather different aspects of the generating processes are emphasized by the sampling procedures of these two sets. Internal wave interpretations will now be offered.

1. Modulation amplitude scaling. In view of the theoretical concepts developed in section A of this chapter, the displacement data of E-3 suggest that, over short time scales, the internal wave field displays one or more of the following features: 1) broadband frequency content, 2) many vertical modes operating, or 3) vertically propagating wave trains. Any combination of these would result in ensemble data where the identity of individual vertical cycles is lost but the dependence of amplitude on stratification would cause a modulation according to (IV.A.8).

For wave frequencies much less than the local buoyancy frequency, the displacement amplitude should scale with $N^{-1/2}$,

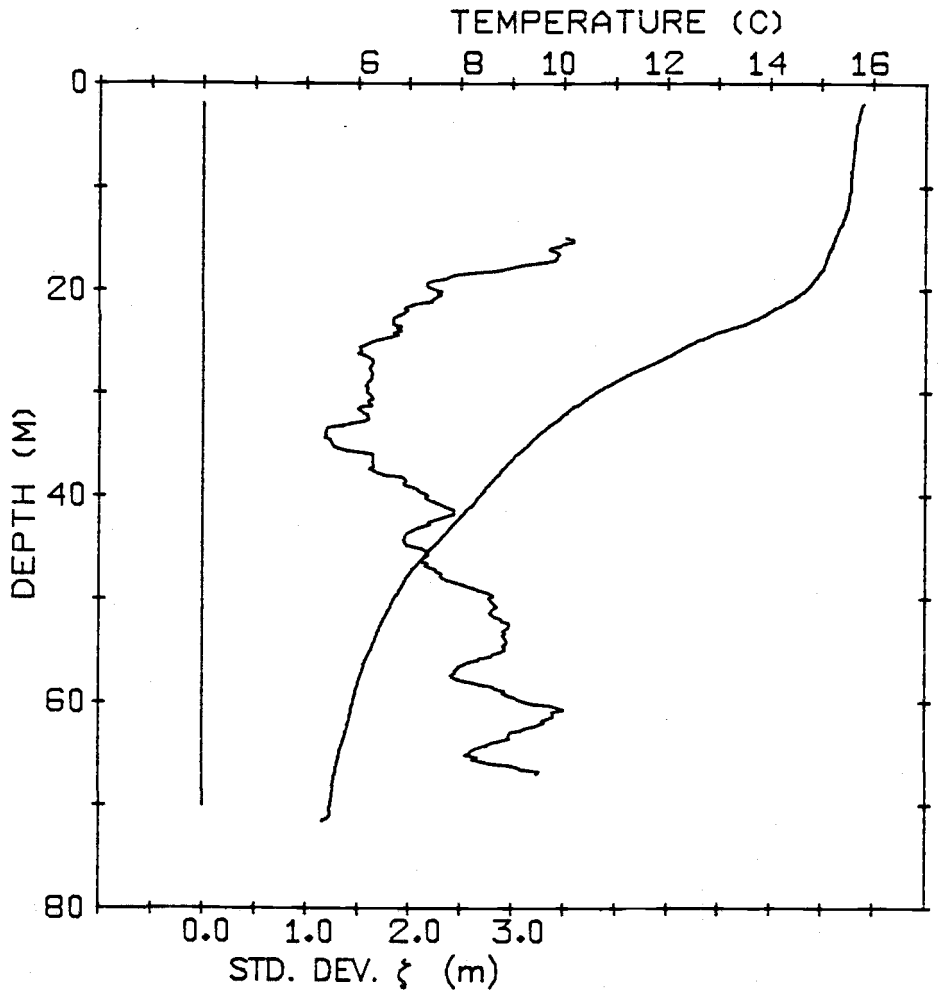

Figure IV.1(a) Ensemble standard deviation displacement profile for the station ensemble (E-1).

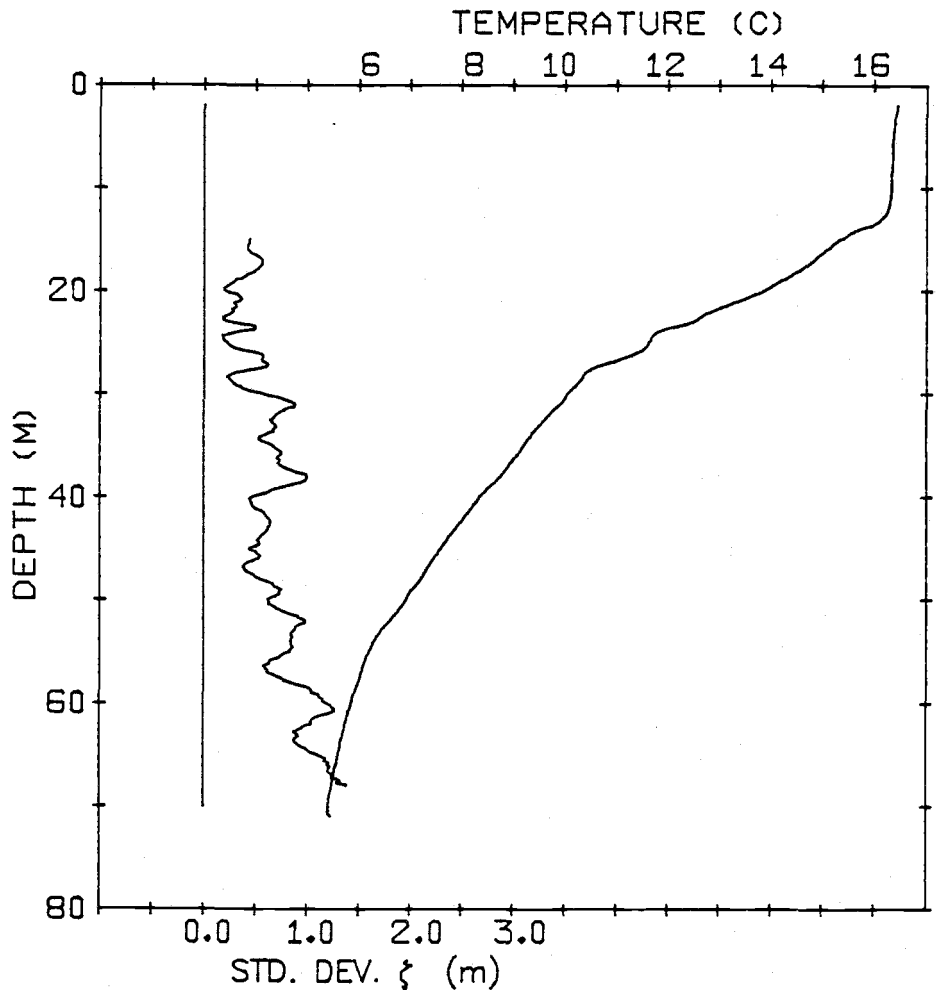

Figure IV.1(b) As in (a), but for the local ensemble (E-3).

i.e., $N^{1/2}s_\zeta$ should be independent of depth. This (WKB) scaling is shown in Figure IV.2 and it appears to have successfully removed the trend that was apparent in Figure IV.1(b). Thus, the data are consistent with generation by internal waves of the sort described above. Considering the sampling filter, these waves must have had periods no greater than a few hours; their rms displacements were less than 1 m over most of the measured portion of the thermocline.

For one of his North Pacific data sets, Gregg (1977) applied the above scaling to displacements in the main thermocline and found it did not render them stationary in depth. In addition to covering a much greater depth range than the Lake Tahoe measurements, his ensemble differed from the present one (E-3) in that it was spread over a two week period.

2. Low order, vertical modes. The displacement variability in E-1 inspires a rather different interpretation than that given for E-3; clearly WKB scaling would not remove the large scale vertical structure observed in Figure IV.1. Consider, however, the displacement pattern that would be produced by internal waves composed of a small number of low order vertical modes. At a given frequency, the nodes and antinodes of each mode of $Z(z)$ correspond to specific depths. Moreover, for low order, low frequency modes, the depth interval of our thermocline data will be less than a wavelength. So, rather than depth-dependent

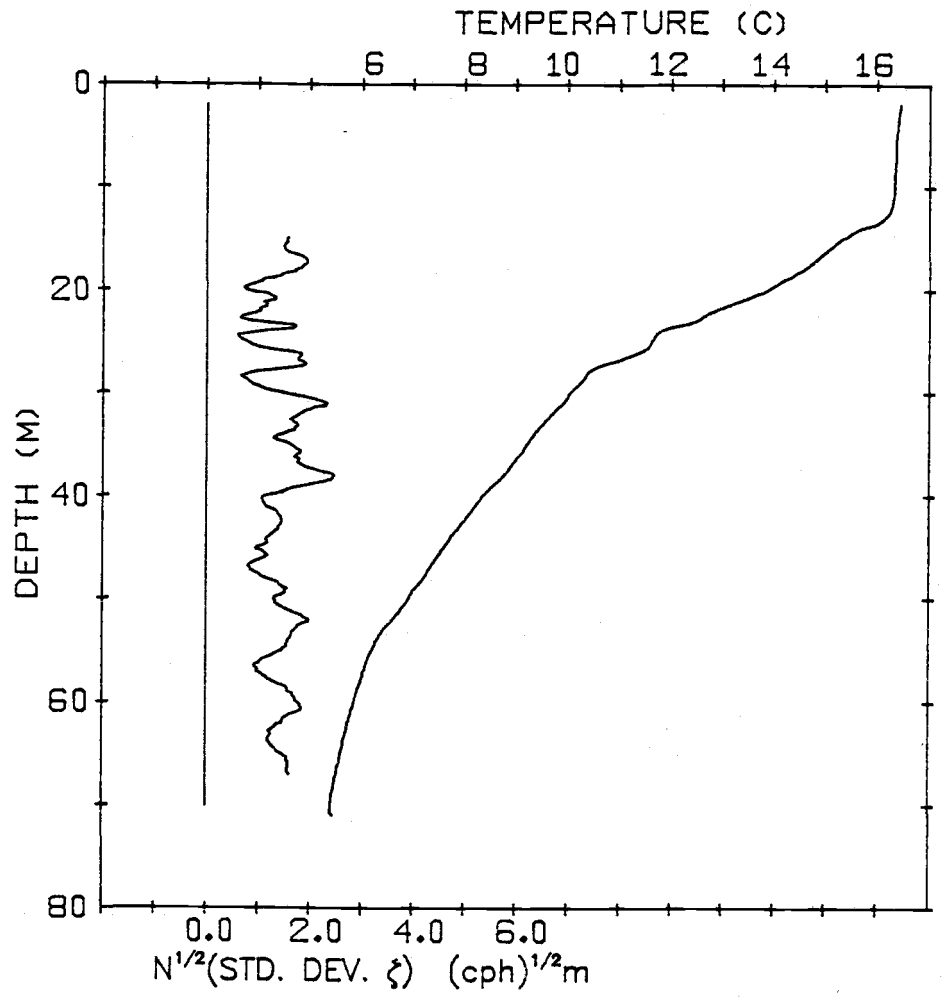

Figure IV.2 Profile of WKB-scaled displacements for the local ensemble (E-3).

modulation, the displacement record would reflect, instead, the structure of an individual vertical cycle of Z. The picture becomes less distinct with greater modal and/or frequency content. However, frequency spectra of internal waves displacements are usually quite red (Cairns, 1975) so, if the energy of the low frequency motions is concentrated in a few modes, then a modal interpretation of the ensemble displacements should be appropriate.

Numerical solutions of (IV.A.5), subject to Z = 0 at the top and bottom of the water column, were obtained with the aid of software written by Dr. Murray Levine. For the upper 70 m, N(z) was derived from the ensemble mean temperature profile as in Figure III.8. Below that, it was assumed to decay exponentially with an e-folding depth of 300 m. Since a strong 12 hour periodicity was observed by Dillon and Powell (1979) in current meter records from the upper 26 m, the corresponding frequency was specified in (IV.A.4).

The first three modes (eigenfunctions) are shown in Figure IV.3. Zero crossings for the second and third modes occur in the upper thermocline, near enough to the minimum of s_ζ to warrant pursuing their association a bit further.

At a given horizontal location, which may be taken as x = 0, the total vertical displacement due to modal internal waves of frequency ω, will be

$$\zeta(0,z,t) = \sum_n a_n Z_n(z)\exp(i(\omega t + p_n)) \qquad \text{(IV.B.2)}$$

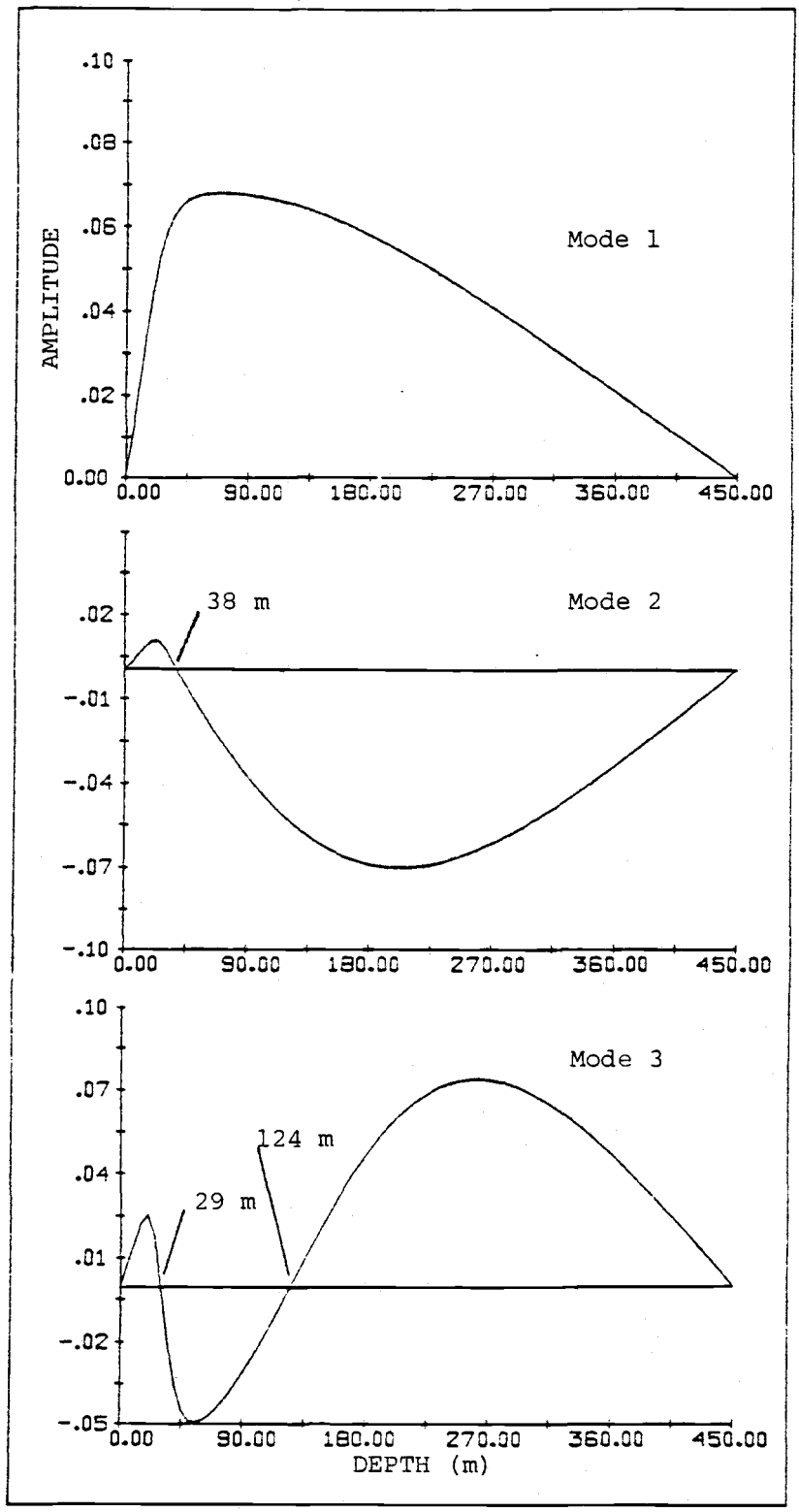

Figure IV.3 Three lowest order vertical modes for the vertical displacement wavefunction at a 12-hour period.

where n specifies the mode number, a is the amplitude coefficient of the normalized eigenfunction Z, and p_n is the phase constant. Over the three week ensemble, it may be assumed that many realizations of each mode contributed to the displacements at this location. Assuming no correlation among the phase constants of any realization of any mode, the cross terms in the mean square of (IV.B.2) will have no net effect, leaving

$$\overline{\zeta^2}(z) = \frac{1}{2} \sum_n a_n^2 Z_n^2(z) \qquad \text{(IV.B.3)}$$

Using the three modes in Figure IV.3, a synthetic s_ζ profile was obtained from the square root of (IV.B.3), with $(a_1, a_2, a_3) = (25, 145, 60)$. This is represented as the dashed line in Figure IV.4 superimposed on the s_ζ data. Below about 20 m, away from direct mixed layer influence, the large vertical scale structure of s_ζ is well represented by the internal wave displacement curve.

C. Discussion of the modal interpretation.

This modest success does not, of course, validate this particular three-mode composition as a unique, exact description of the low frequency motion in Lake Tahoe. For a somewhat different frequency, other, equally good, low mode weights could probably be found. Furthermore, three weeks of possibly non stationary data are lumped together in this ensemble of profiles.

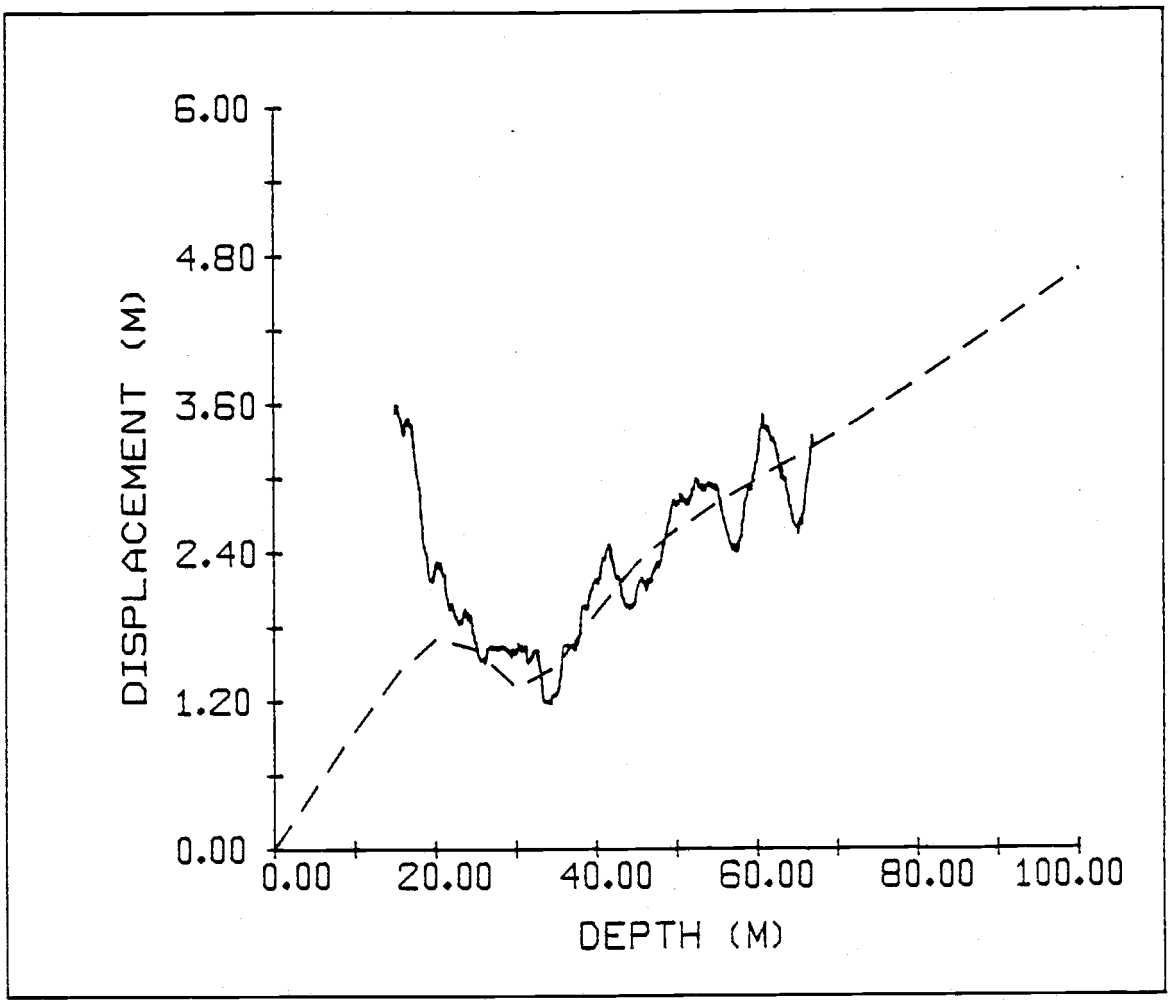

Figure IV.4 Root-mean-square vertical displacement profile due to random-phase realizations of the three 12-hour modes, superimposed on the ensemble displacement profile of E-1.

Still, the evidence supports the interpretation that some combination of low frequency, low order mode internal waves contributes significantly to the observed variability in the upper thermocline and that these waves impart some modal character to the vertical structure of that variability.

Of particular importance is the fact that the lowest mode, acting alone, cannot account for the conspicuous local minimum in temperature variance at 35 m in the station and transect ensembles. Theoretical models make frequent use of a two-layer approximation (two superposed fluid layers, each of constant density) as the simplest representation of stratification in lakes and oceans. In recent review articles, Csanady (1975) and Mortimer (1974) used such models extensively in analyzing lake dynamics and, to be sure, a considerable amount of the physics of stratified fluids can be learned this way. Many of the theoretical results are qualitatively consistent with lake observations. The same applies to oceanic research.

But there are limitations to the two layer idealization; one is that it allows only one internal mode. The present results suggest that an important, perhaps dominant, role is played by some higher order mode(s) in the generation of temperature fine-structure (transient finestructure associated with internal wave displacements). Csanady (1968, errors corrected by Birchfield, 1969) has studied theoretically the motions in a circular, two layer model of constant depth, with dimensions appropriate to the

Great Lakes. He then generalized the stratification somewhat (Csanady, 1972) by inserting a third layer, with linear density structure, between the top and bottom homogeneous layers. Although some general features of the two layer model results were virtually unaffected by the presence of the more realistic thermocline, important additional features were found, namely significant excitation of the second and third vertical internal modes by impulsive wind forcing.

I have emphasized the qualitative nature of the modal interpretation; the present data set justifies no more. Still, some rough checks of consistency are in order. Horizontal velocities may be estimated from the displacement modes through (IV.A.2) and (IV.A.6). Beneath the shallow antinode of mode 2 (Figure IV.3) the vertical gradient is fairly constant and corresponds to a horizontal current amplitude of about 3 cm/s. In the same depth region, mode 3 makes a comparable contribution, whereas mode 1 has a negligible horizontal velocity. As averages over the three weeks, these magnitudes compare favorably with the currents measured in the thermocline by Dillon and Powell (1979).

Horizontal wavelengths of the three 12 hour modes are 25.6, 11.6, and 7.7 km, and phase speeds are 59, 27, and 18 cm/s. The shape of Lake Tahoe at the 200 m isobath is approximately rectangular, 13 by 27 km. Thus the waves will be strongly influenced by the horizontal boundaries. In fact, for simple seiches

(neglecting Coriolis effects), the two lowest vertical modes fit rather well as first and second transverse modes, or as second and fourth longitudinal modes. The third vertical mode, least affected by the boundaries, happens to fit as the seventh longitudinal mode but little importance should be attached to an assignment of such high modality when using these approximate numbers. In any event, true basin modes will be modified somewhat by the earth's rotation. Computation of free mode structures and frequencies in a rotating rectangular basin is not straightforward analytically. See Rao (1966) for some numerical solutions and the interesting history of work on this problem.

D. Scaling the temperature spectra.

Continuing the interpretation that the observed temperature variability was due to internal wave vertical displacements (IV.B.1), we now consider the vertical wavenumber spectra of temperature fluctuations, described in section III.F, in that light. It is common, and consistent with the stated interpretation, to simply divide such a spectrum by the square of the mean temperature gradient (Hayes et al., 1975) to estimate the spectrum of displacements, and that procedure is followed here. Gregg (1977) used it as well, but he also demonstrated that, for one of his data sets, the resulting spectrum differed somewhat at the higher wavenumbers from a spectrum of more directly estimated displacements.

The validity of the procedure may certainly be doubted when the temperature gradient varies substantially over the depth interval for which the spectrum is computed. For that reason, we restrict the practice here to the short interval spectra that were shown in Figure III.10.

Using the mean gradients in Table III.3, the temperature spectra of E-1 and E-3 were scaled and the results appear in Figure IV.5. Whereas the four individual temperature spectra of E-1 varied in level by a factor of 20 to 30, the associated displacement spectral levels differ by less than a factor of two over most of the band.

The effect on the E-3 data was much the same for the three deeper intervals; the collapse is not quite so tight as for E-1 but the variation is comparable to the 95% confidence intervals of the original spectra. The spectrum for the 25 m interval is considerably lower than the others at small wavenumbers, but joins them above about 0.6 cpm. The departure must somehow reflect the influence of the prominent, thin mixed layer described in section III.D. It evidently inhibited the amplitude of the large scale displacements, but on average, over the analyzed interval, the smaller scale activity was about the same as it was in the deeper water. Exclusive of this anomaly, the inferred displacement spectra of both ensembles are stationary in depth over the wavenumber band shown (more precisely, with the present data, this statement cannot be rejected).

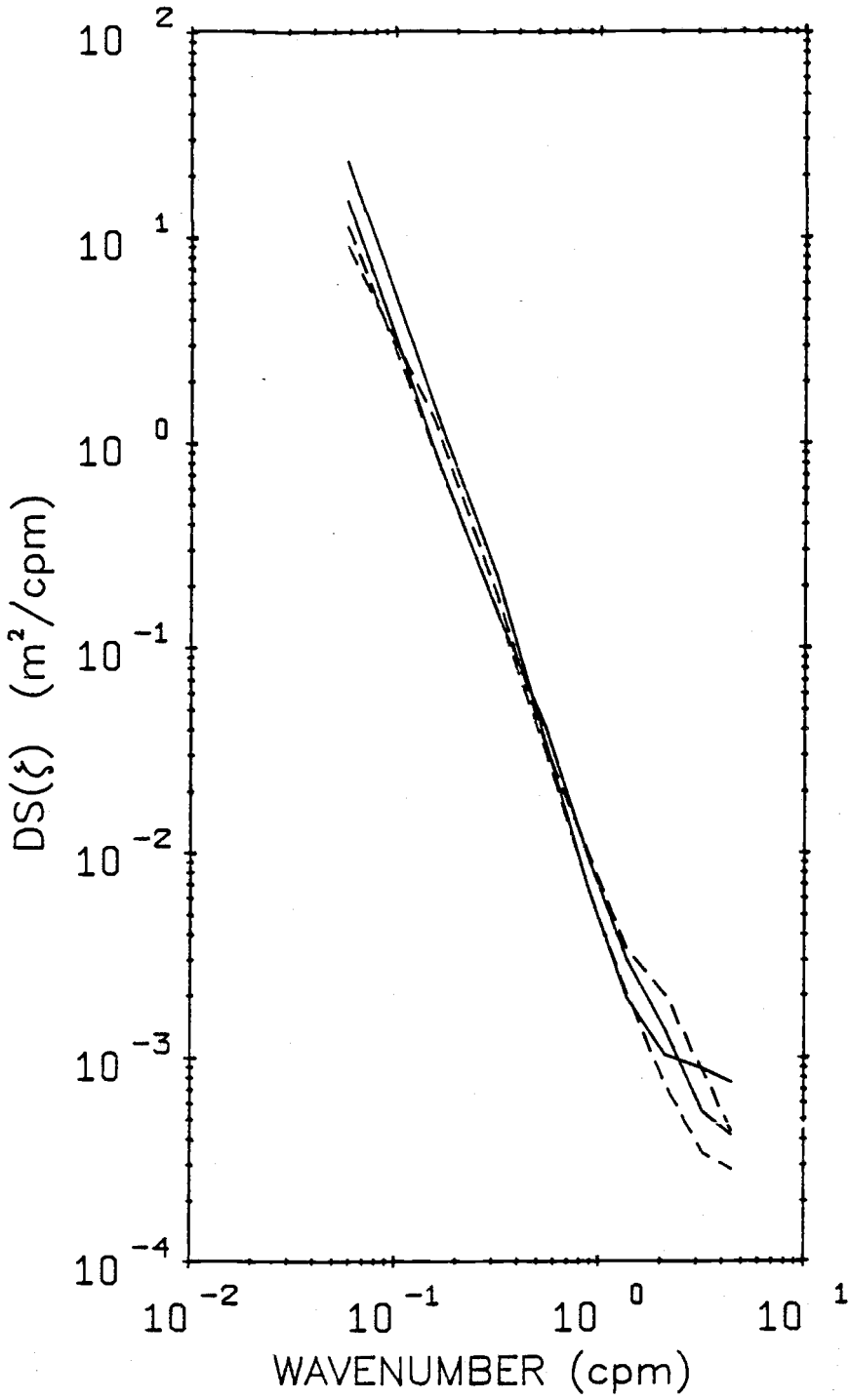

Figure IV.5(a) Displacement spectra for E-1, formed from the temperature spectra of Figure III.10(a). DS denotes dropped spectrum.

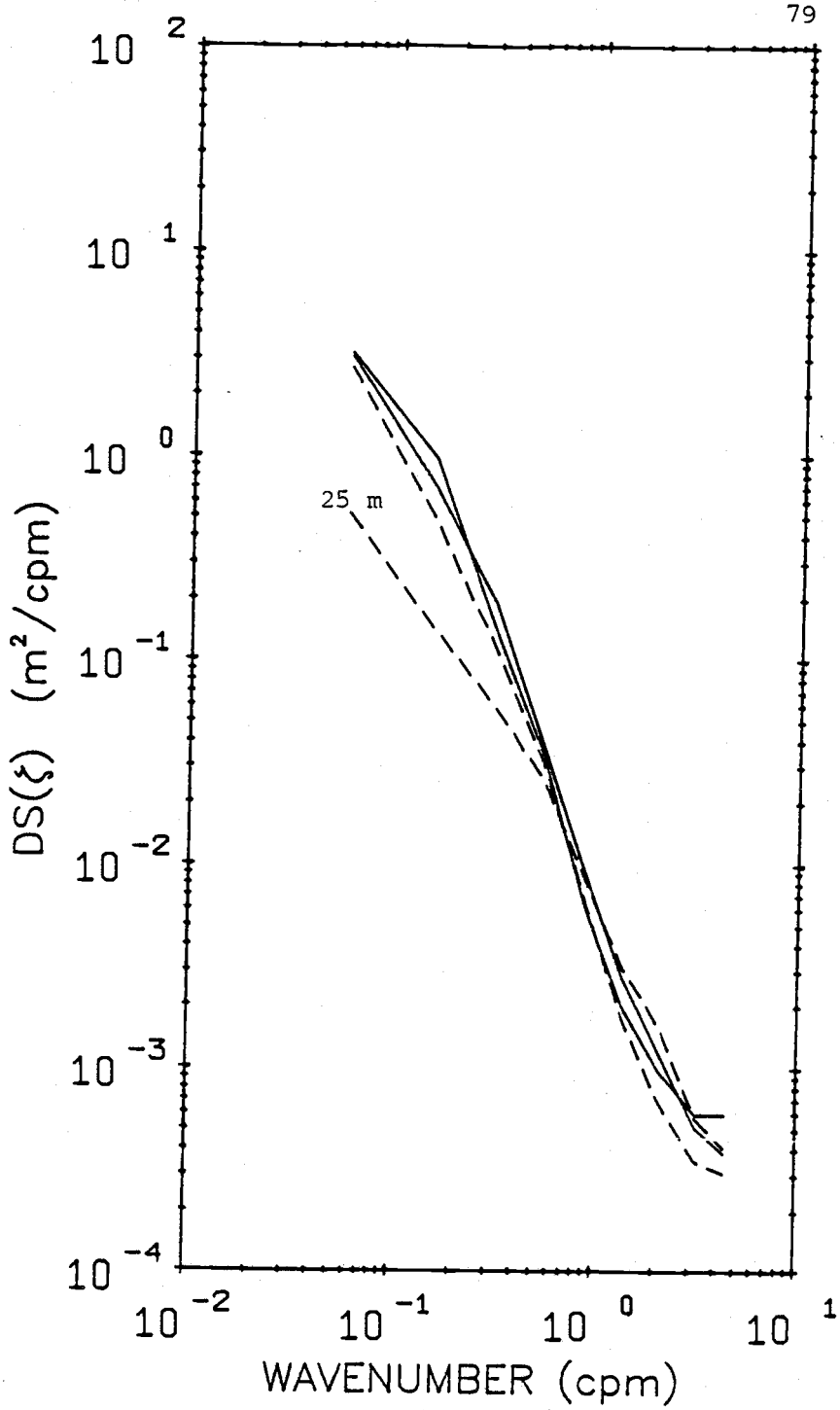

Figure IV.5(b) As in (a), but for E-3 (cf. Figure III.10(b)).

Consider now the vertical wavenumber spectrum of internal wave vertical displacements. As shown in section IV.A, if m(z) is slowly varying, and if the wave frequency is much less than the local buoyancy frequency, two effects bearing on the spectrum occur: the displacement amplitudes scale with $N^{-1/2}$, and the wavenumber scales with N. Then, as Phillips (1977) explains, if the displacement spectral density is multiplied by N^2 and plotted against m/N, the result should be independent of depth. So-scaled spectra are shown in Figure IV.6 for E-1 and E-3.

Observe that, with the lateral shift effected by the wavenumber scaling, there is a narrower band over which the spectra may be compared. For E-1, the three shallower spectra may be considered stationary but that of the 54 m data interval is separated beyond overlapping confidence intervals. For E-3, the three deeper spectra are well collapsed, but the 25 m spectrum retains the independence it exhibited in Figure IV.5 (in fact, for the WKB-scaled spectra it is separated over a greater wavenumber band).

It is interesting that Hayes et al. (1975) observed very similar effects on their Atlantic temperature spectra, when scaled in the two ways discussed here. Specifically, both the displacement and the WKB scaling caused a strong collapse of the spectra; from his Figures 5 and 6 it would seem that the WKB scaling was slightly the less effective of the two. With the displacement scaling, the Lake Tahoe spectral levels are about 0.3 to 0.5 times as great as

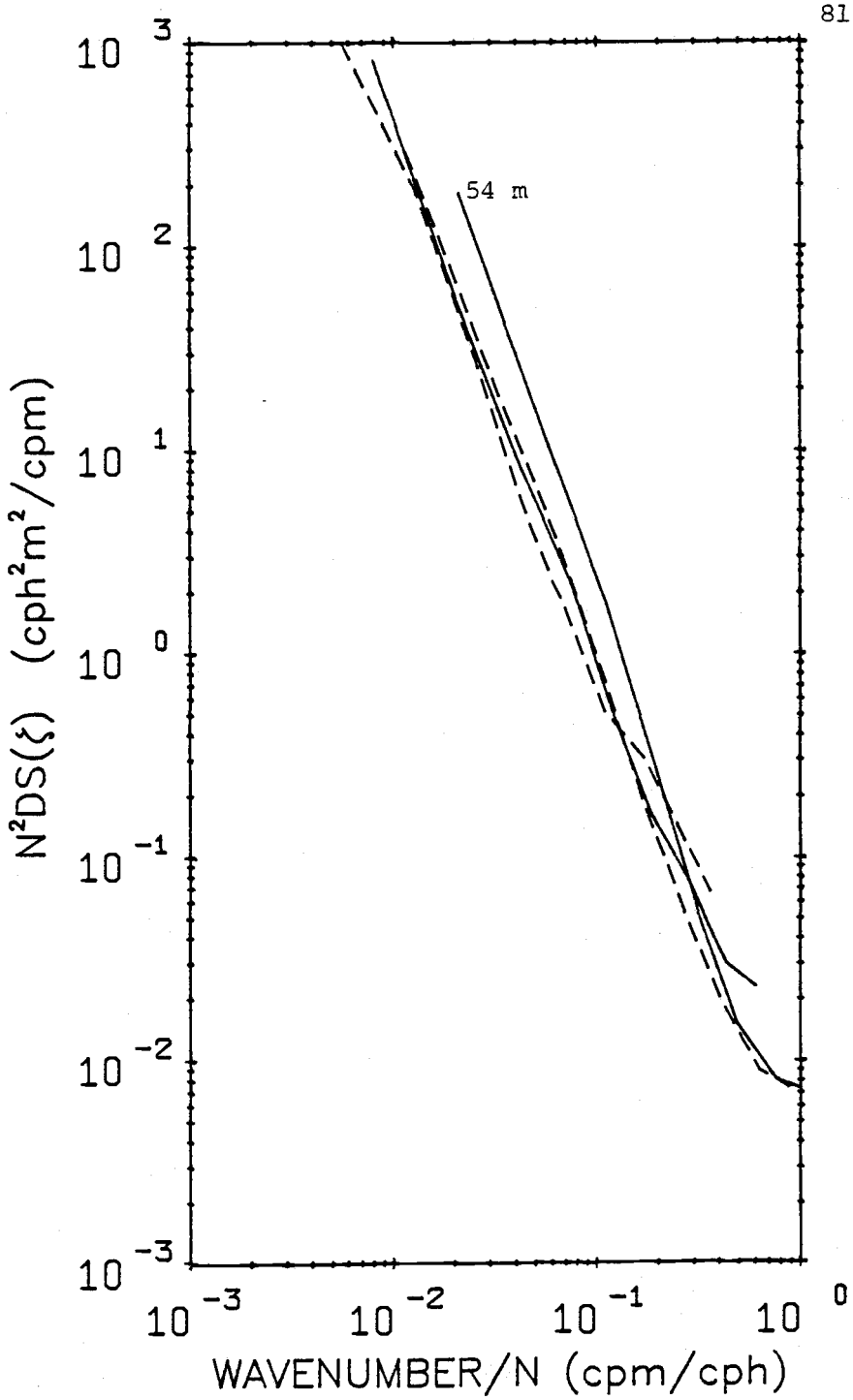

Figure IV.6(a) WKB-scaled spectra for E-1.
(DS denotes dropped spectrum)

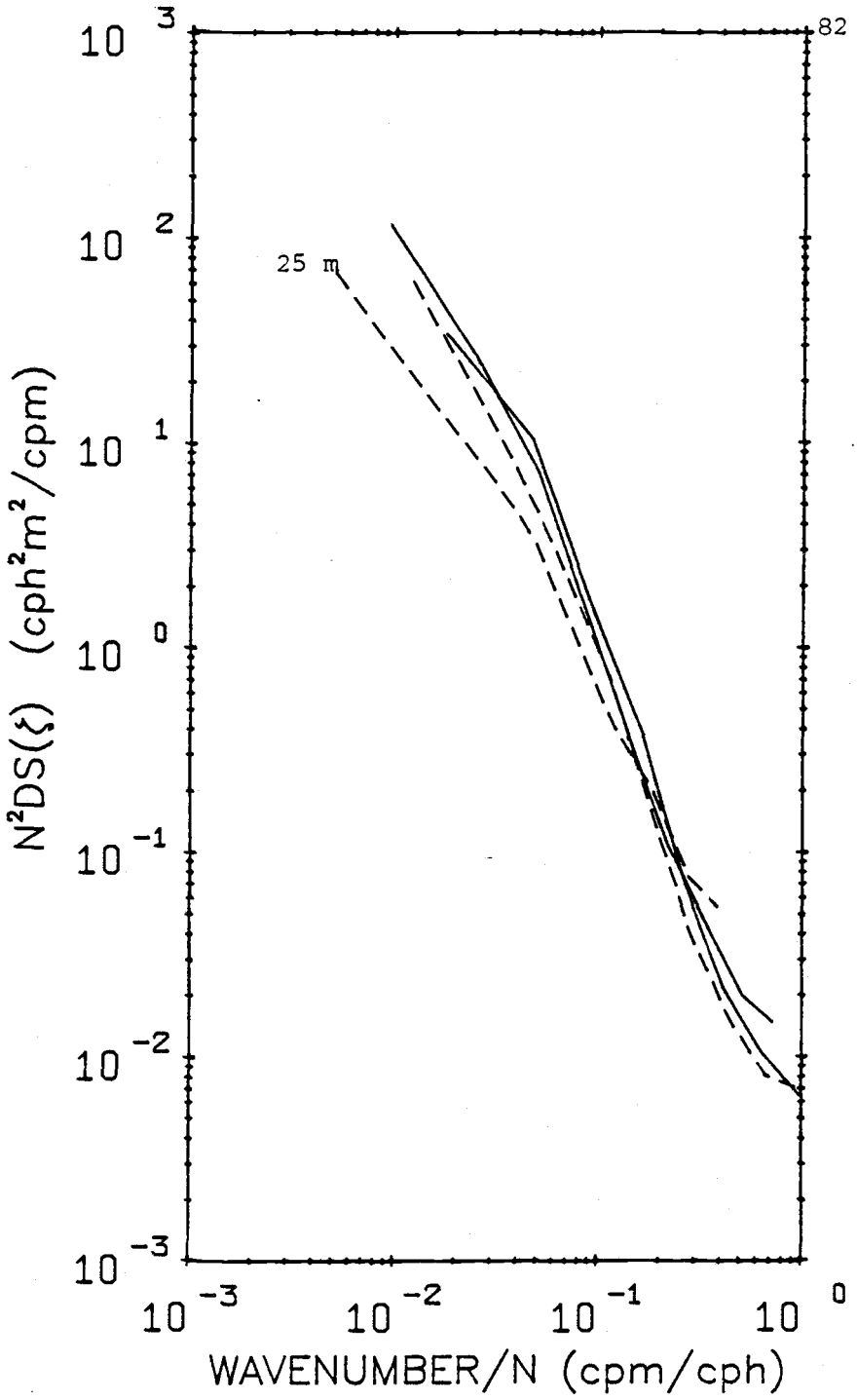

Figure IV.6(B) As in (a), but for E-3.

the Atlantic levels over the decade 0.1 to 1.0 cpm (and up to 0.7 times as great as some of the main thermocline spectra reported by Gregg (1977)).

The similarities of the Tahoe results to those of Hayes et al. (1975) should be considered alongside some of the vast differences of the data sets. The buoyancy frequency range for the lake profiles was 13 to 2.5 cph; for the Atlantic profiles it was 2.6 to 0.4 cph. The deepest and shallowest depth intervals analyzed were centered at 54 and 25 m at Lake Tahoe, and at 5200 and 350 m at the Atlantic site. Horizontal domains are a 20 km enclosed basin compared to the open ocean, and total water depths differ by an order of magnitude. And within the measured portion of the Tahoe thermocline, the e-folding length scale of the buoyancy frequency is only 20 m. Yet temperature fluctuations throughout both data sets, over more than a decade of vertical scales, possessed similar spectral shapes. Further, when scaled by local temperature gradients, these spectra collapsed, not only for each data set but for both of them, to within a factor of four of the same spectral level. To the extent these scaled spectra really represent vertical displacement spectra, we may conclude that the physical processes that generate and control these displacements operate very uniformly over an extremely large range of environmental parameters.

E. The cross spectra.

In presenting the horizontal-temporal coherence results

(section III.G), we referred to the work of Hayes (1975) and Stegen et al. (1975) and noted some similarities in coherence behavior, but the settings were quite different. In vertical regime (upper thermocline) our data is more akin to Stegen's although the vertical ranges were quite different. Also, our largest horizontal separations were about the same as his smallest. The Hayes data were collected in the permanent thermocline and over a much greater time interval than ours, although, for one of his data sets, the horizontal area was of the same order as ours. Thus, the Tahoe results may be regarded as the first description of coherence in the temperature perturbation field over the present space-time scales.

The relative importance of temporal and horizontal separation is not known for our coherence results. However, consider the following generalization of some ideas expressed by Hayes (1975), who was considering only the temporal effects. If the temperature variability is associated with internal wave displacements, and if the vertical structure is modal, then the coherence and phase dependence on $p = k\Delta x - \omega\Delta t$ is predictable (for a particular frequency and horizontal wavenumber) where Δx and Δt are the horizontal length and the time separations respectively. If the process is well sampled, the coherence will fall from one to zero as p goes from zero to $\pi/2$ while the phase is constant at zero. For p between $\pi/2$ and $3\pi/2$, the phase will be 180° and the coherence will rise to one at $p = \pi$, falling to zero again at $p = 3\pi/2$.

In Figure III.12, for the 6.5 m wavelength, the coherence and phase behavior is quite like that just described, although one might like to see a little more precipitous phase jump. At 13.5 m wavelength, the coherence hits a minimum a little later, so the phase reversal should start later, which it does, but seems stalled at about 100^{o}.

Many factors may conspire to prevent the predicted behavior from showing up plainly in real data. A realistic band of frequencies and horizontal wavenumbers, and propagating rather than modal vertical structure are among these. Also, we have no information on the relative directions of the boat drift, horizontal mean currents, and wave propagation. Current meter measurements would help in future work, and a longer series of profiles might reveal additional phase reversals and coherence zeroes.

F. Summary.

In this chapter, many features of the finestructure temperature observations have been found to be consistent with the interpretation that the variability was due to internal waves distorting the mean temperature field.

The rather different standard deviation profiles of the station (E-1) and the local (E-3) ensembles can be explained by the following composition of internal waves. Over the longer time scales of E-1, the internal wave field is dominated by a few, low order vertical modes with periods of roughly 12 hours. Since the horizontal scale of these waves is not small compared to the basin dimensions, their horizontal structure is presumably modal as well. Zero crossing depths in the second and third vertical modes correspond to the observed minimum in temperature variance. In the present study, only the transient, wavelike variability of these low mode waves was considered. It is possible that shear instability of these waves plays an important role in vertical transport processes as well. Since vertical shear has a zero crossing at the same depth as vertical displacement, there could exist depths of reduced mixing potential. The present data set did not permit verification of this concept; it remains an intriguing possibility of considerable significance.

Over the shorter time scales of E-3, these slow waves were effectively filtered out, leaving the higher frequency, smaller-scale

waves. Displacements inferred from the temperature data of E-3 suggest that the small-scale wavefield has one or more of the following: 1) broadband frequency content, 2) many vertical modes active, or 3) vertically propagating packets. Furthermore, the E-3 displacements scale with depth in the WKB sense, also consistent with the wave interpretation.

The temperature spectra of Chapter III were scaled as spectra of vertical displacements and also to account for the wavenumber and amplitude changes (with depth) appropriate for small-scale internal waves (WKB scaling). In general, both scalings were highly effective in collapsing the original temperature spectra. Remarkably similar results were reported by Hayes et al. (1975) with data from the Atlantic Ocean. Not only were the effects of scaling similar in collapsing the separate sets of temperature spectra, but the displacement spectral levels from Tahoe were lower than the Atlantic levels by only a factor of 0.3 to 0.5.

The coherence and phase behavior as a function of separation in the local ensemble (E-3) is somewhat suggestive of a vertical modal structure for the small-scale waves (this proposition is unrelated to the modal interpretation given above (and in Section IV.B) for the large-scale structure in E-1).

Finally, it was remarked at the end of Chapter III that Tahoe might make a good physical oceanography laboratory for studies of small-scale dynamics. The results of this chapter throw additional light on that concept. Variability in Lake Tahoe on time scales

greater than a few hours may be dominated by internal wave motion related not only to the stratification (and wind regime), but to the basin dimensions as well. However, over vertical scales of 1 to 10 m, corresponding, presumably, to higher frequency motion than the basin modes, the temperature variability in Lake Tahoe has much in common with that in the oceans. Thus the lake holds great potential as a field site for investigations of internal waves and mixing.

CHAPTER V. VERTICAL MICROSTRUCTURE OBSERVATIONS

In this chapter, we pass into a realm of smaller scales and look at some results from the data obtained with the microstructure profiler (MSP, see Chapter II). Regrettably, much of this data was found to be contaminated at the higher frequencies due to an insidious noise problem of which we were unaware at the time the measurements were made. This prevented analysis of the smallest, dissipative scales in the temperature field.

Oceanic investigations with the MSP by Caldwell (1976) and Marmorino and Caldwell (1978), and work with other free-fall profilers (for example by Gregg, 1976), have provided sufficient background that patterns have begun to emerge. A conceptual interpretation of wavenumber spectra of temperature gradients has been suggested by Caldwell, Dillon, Brubaker, Newberger, and Paulson (1979) wherein the observed spectrum is assumed to represent the combined effects of finestructure, turbulence, and noise. Any one component may dominate a particular spectrum, depending on the nature of the structure passed through and on the relative strengths of the temperature signal and the noise. Unfortunately, in the Tahoe MSP data the noise component was often significant above 10 Hz. The corresponding wavenumber band (100 cpm and above, at a drop speed of 0.1 m/s) contains important information for the quantitative analysis of microstructure data. In particular, the methods for estimating kinetic energy dissipation rates, described by Caldwell et al. (1979), could not be used with the Tahoe records.

The general variability of microstructure activity over the data set is adequately represented by plots of temperature and temperature gradient for various profiles. A few of these are presented in the following section; from them, several features of mixing activity can be inferred. In section B, results from MSP drops with two horizontally separated thermistors are discussed.

A. General variability.

Results of a typical microstructure drop are shown in Figure V.1. The presence of microstructure, indicated by the gradient record, is highly intermittent in the vertical. This is characteristic; intermittence was reported in many of the papers cited at the beginning of this chapter (see also Turner, 1973, and Phillips, 1977). One must use caution in interpreting the gradient plots, since regions of small scale temperature variability do not necessarily correspond to active turbulence, but may represent structures remaining after the turbulence died ("fossil turbulence"). At the same time, intense turbulence in an isothermal region will leave no signature in temperature data. Still, a microstructure patch indicates a mixing site, active or not; and a lack of microstructure at a depth where the mean gradient is measurable, implies no strong turbulence or mixing there.

On 9 September (Figure V.1), the epilimnion contained an interface at about 7 m, representing the depth to which some previous mixing had penetrated. The microstructure associated with this

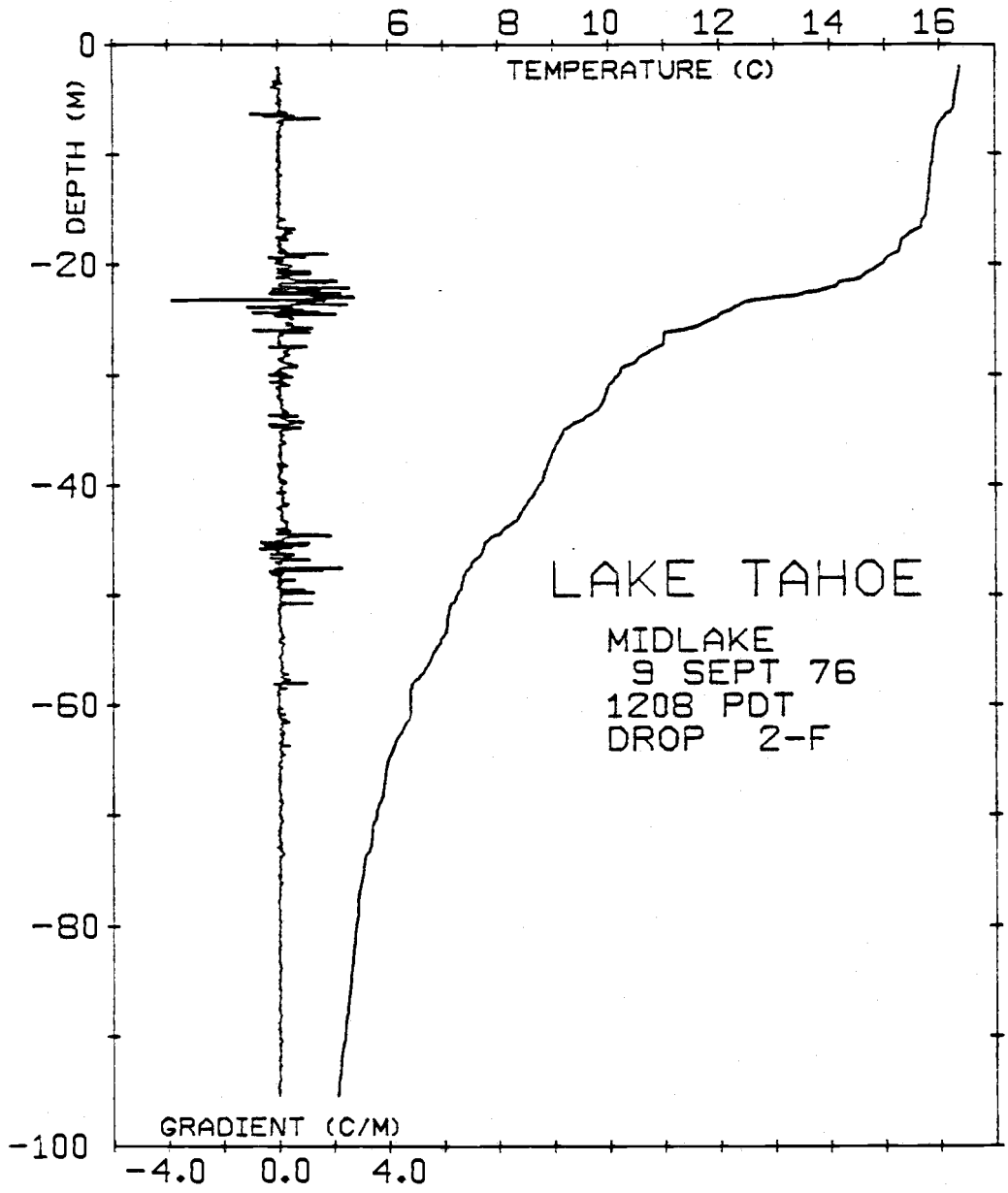

Figure V.1 Microstructure drop 2-F, illustrating general vertical variability of small-scale variance.

interface is quite limited in vertical extent, indicating a lack of vigorous entrainment of fluid from either side of the interface to the other. However, the gradient symmetry suggests at least some exchange. In the deeper patches there are frequent microscale inversions as well, although the overall record is rather positively skewed (note, on the ordinate, that z has been taken as positive upward, so that positive temperature gradients are stable).

In one of the quieter records, shown in Figure V.2, there are virtually no inversions on any scale, the series of positive gradient peaks corresponding to an inactive, steppy structure. Figure V.3 illustrates the penetration of wind mixing into the shallow, diurnal thermocline.

Observations of boundary-induced mixing, inferred from a series of MSP temperature records over the lake slope, were reported earlier by Caldwell, Brubaker, and Neal (1978), but we didn't include gradient microstructure data in that paper. Figure V.4 shows the most shoreward profile; note the change in gradient scale. The general level of gradient magnitudes was greater by about a factor of two for this profile than for any midlake MSP record. And at a station just 200 m further from shore than drop 15-D, the microstructure level was considerably reduced from that shown in Figure V.4, indicating that this mixing boundary layer had a very short horizontal scale.

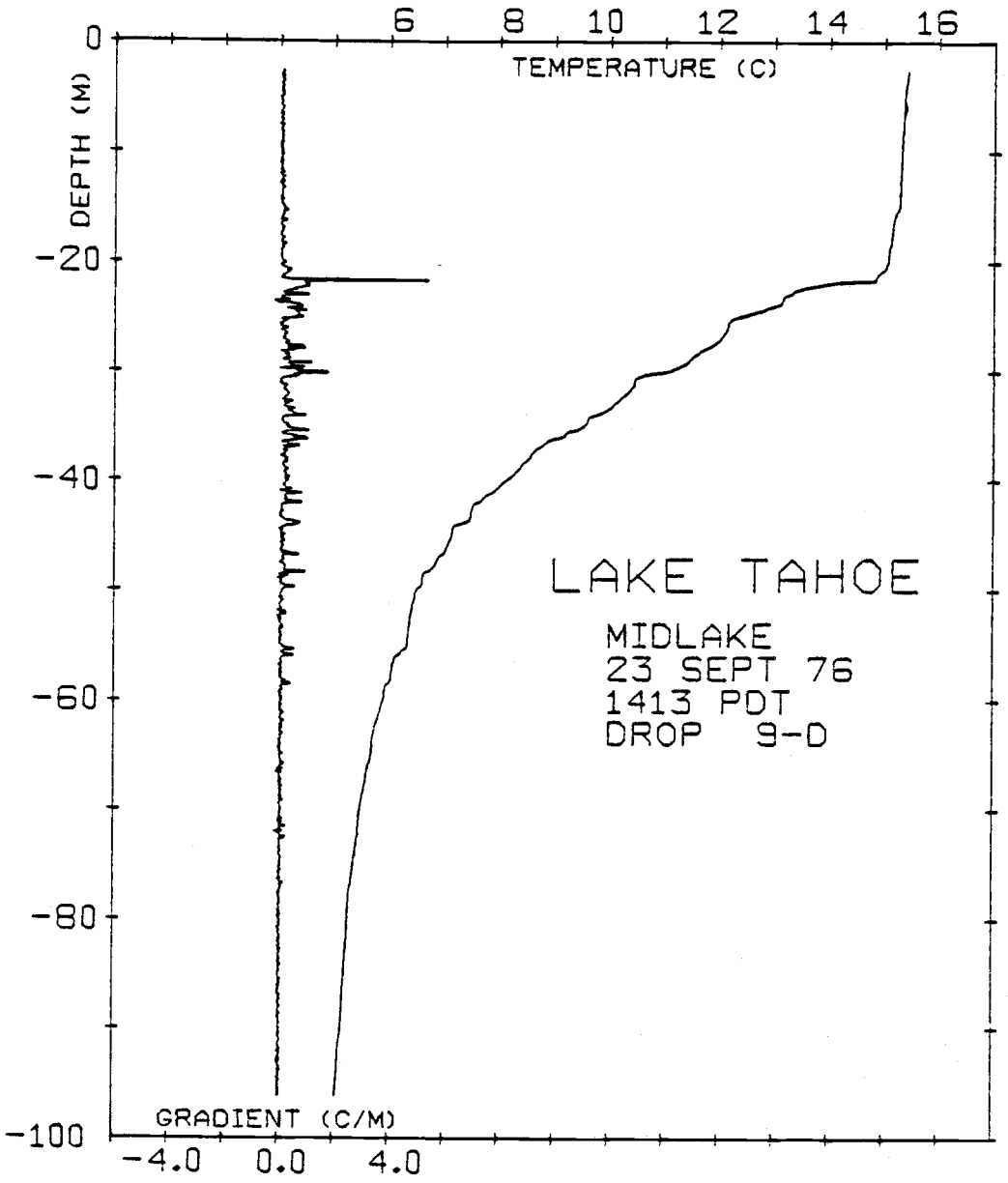

Figure V.2 Microstructure drop 9-D, a "quiet" record in which virtually all the microstructure is positive (stable gradients).

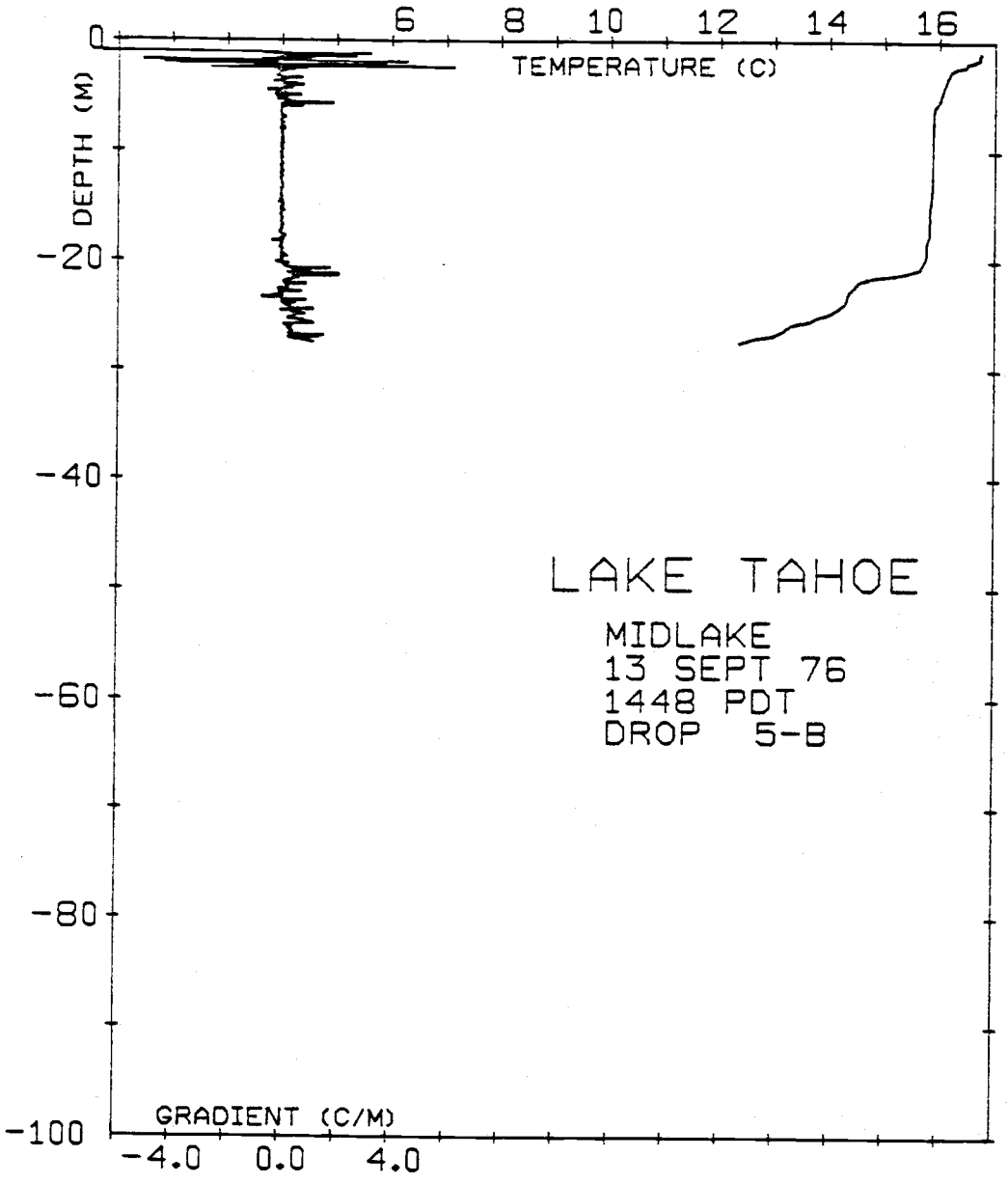

Figure V.3 Microstructure drop 5-B, showing the penetration of mixing activity due to surface forcing.

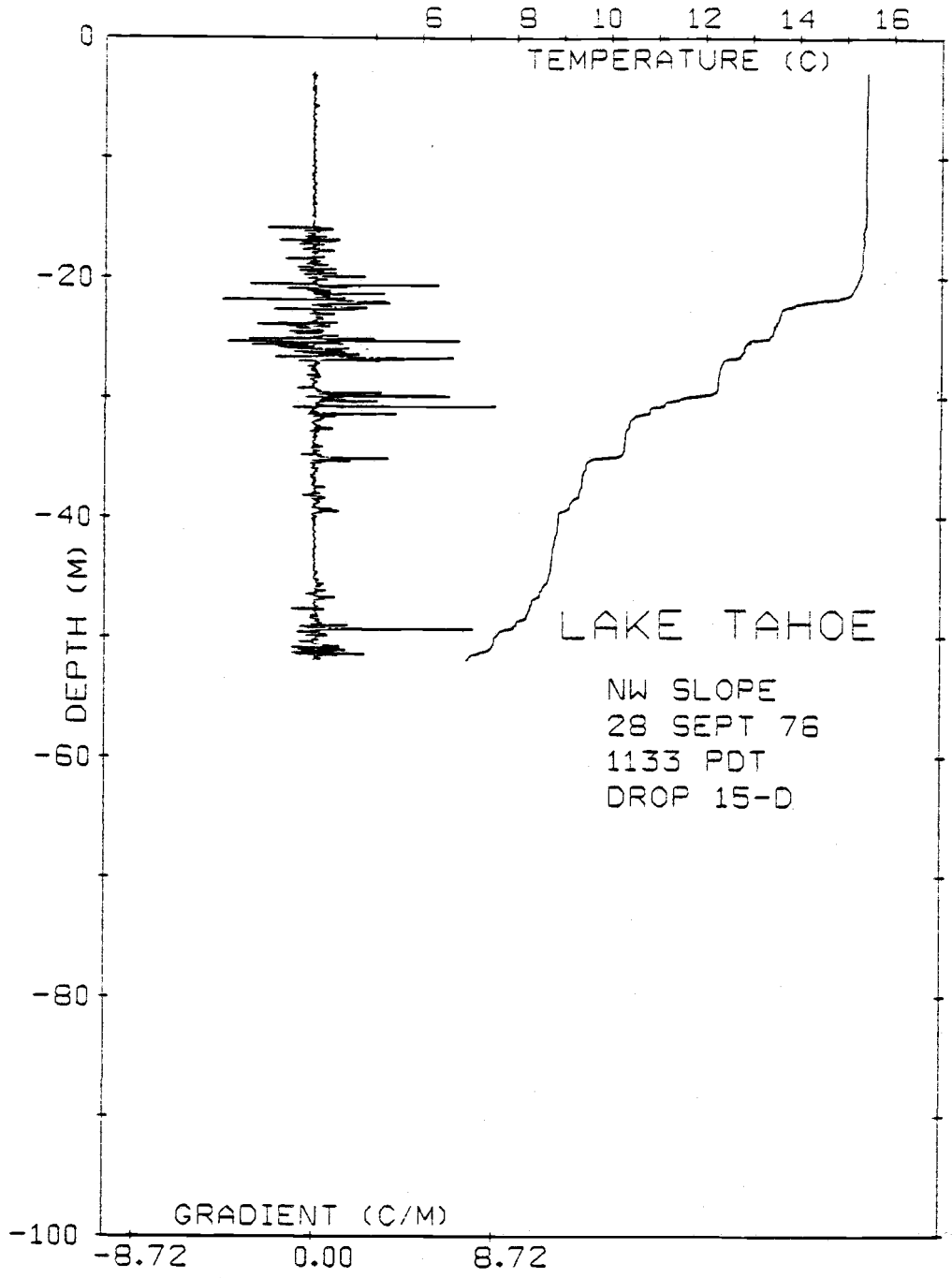

Figure V.4 Microstructure drop 15-D. Increased microstructure level due to slope-induced mixing. The temperature profile shows that the thermocline here is composed of a series of mixed layers of varying thicknesses, separated by high-gradient sheets.

B. Horizontal coherence.

Several MSP drops were made on 25-27 September with two horizontally separated thermistors on the same instrument body. Comparison of the two temperature records provided some information on the horizontal variability of vertical microstructure.

At separations of 3 to 46 cm, many temperature features were present in both signals, even when the vertical scale of the features was smaller than the separation. A horizontally elongated shape for many of the structures may thus be inferred, indicating some degree of anisotropy. Frequently, though, horizontally localized patches were encountered resulting in a very active signal from one sensor, while the other missed it completely. Evidently, the boundaries of patches were occasionally very sharp.

Cross spectra of the two signals were computed over 2048 point gradient series to which a Hanning window had been applied. These series corresponded to 25.6 second segments and about 3 m (vertically) through the water at a drop speed of 0.12 m/s. Coherence estimates were computed from band-averaged cross spectra. Typical thermocline coherence spectra began high at the smallest vertical wavenumbers, fell to an insignificant level at intermediate wavenumbers, and then rose again at high wavenumbers due to the high frequency electrical noise. For horizontal separations to be considered below (3, 23, and 46 cm) an adequate spectral gap usually separated the noise from the low wavenumber, coherent signal, so the coherence

roll-off was well-defined. (Data from drops with horizontal separations of order 1 cm were not usable because the temperature coherence persisted to high enough vertical wavenumbers that it merged with the noise.)

The inverse of the (vertical) radian wavenumber, m_0, at which the coherence squared fell to 0.5 was used to define a vertical scale for features with horizontal scale comparable to the sensor separation, r. The ratio of these scales represents a shape factor or aspect ratio, $A = m_0^{-1}/r$. Since the coherence roll-off was sometimes irregular, m_0 was determined from

$$coh^2(m) = (1 + (m/m_0)^2)^{-1}$$

for several points along the roll-off. For each m_0, the aspect ratio was computed. The mean aspect ratio for each coherence curve is shown in Figure V.5 as a function of depth.

For each separation shown, the aspect ratio is smaller in the thermocline than in the epilimnion (the upper 20 m), suggesting a shape dependence on local (static) stability. Structures in the epilimnion are also more directly influenced by wind and surface waves and are presumably more energetic. A patch was evidently encountered on one drop between 50 and 55 m in which the features 3 cm wide were nearly round.

The aspect ratio determined from a coherence curve applies only to features with widths the order of the sensor separation.

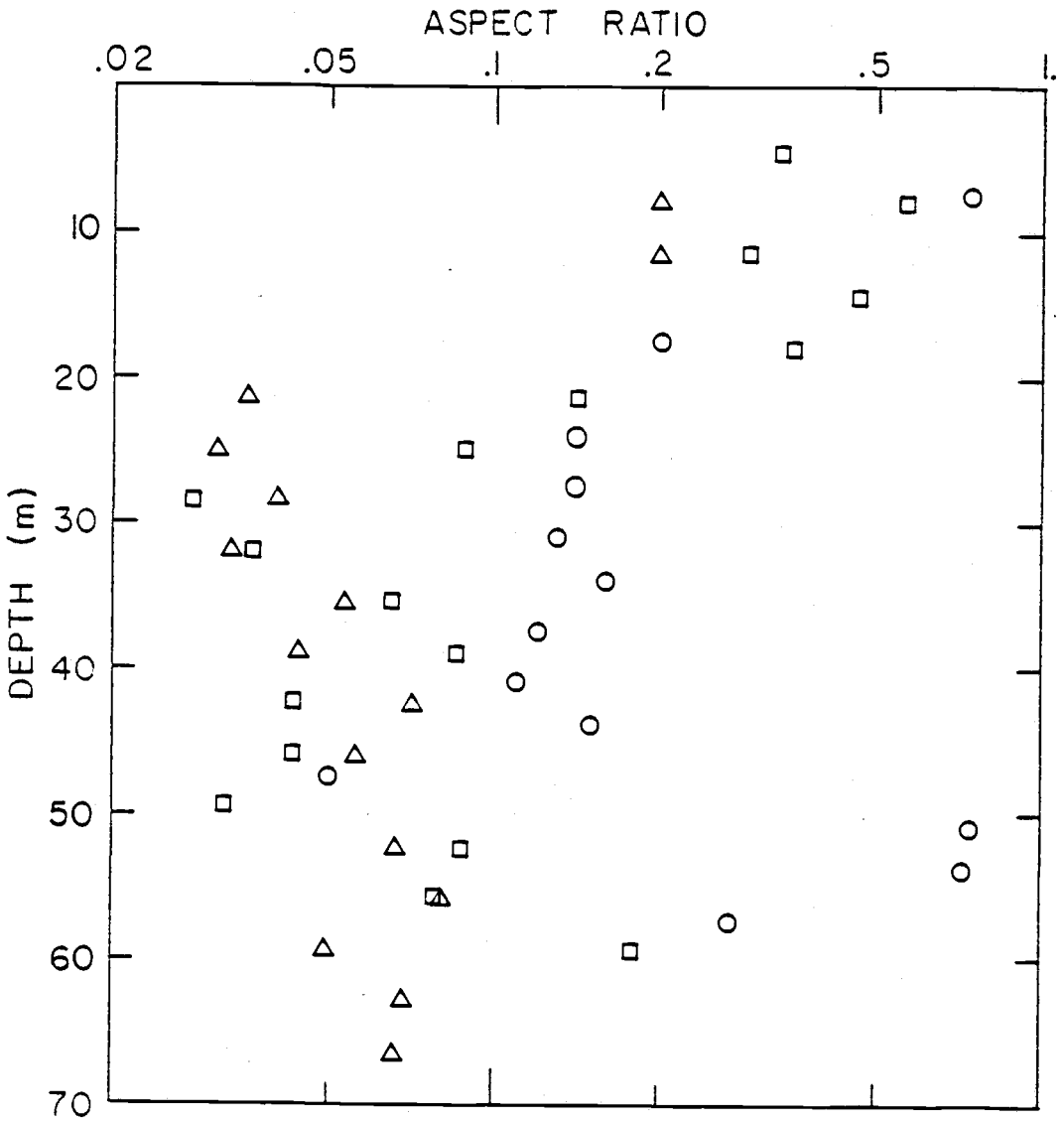

Figure V.5 Aspect ratio versus depth. Separations: ○ 3 cm, □ 23 cm, △ 46 cm.

Figure V.5 shows that, at a given depth, the larger structures are more flattened than the smaller ones. Within the depth interval of 20 to 50 m, the aspect ratios were averaged for each separation and the results are shown in Figure V.6. On each point, the bar indicates the standard error of the mean.

C. Summary.

Despite a serious noise problem, which prevented most of the original objectives of the Tahoe microstructure work from being realized, several observational results on microscale temperature features have been found.

1. Microstructure sites were of limited spatial extent, occupying a small fraction of the total water volume.

2. The boundary between fluid with and without microstructure could be quite sharp.

3. The most active microstructure records were obtained over the steep lake slope in a shore-bound mixing layer. The mean surface water was (of course) the other preferential mixing location, but we were unable to use the MSP during heavy winds to observe the evolution of mixing there with time.

4. Patches of microstructure were observed in the thermocline on most drops, regardless of surface conditions or time since the wind had died, but, occasionally, a record was obtained (Figure V.2) showing generally reduced levels and no inversions of any scale.

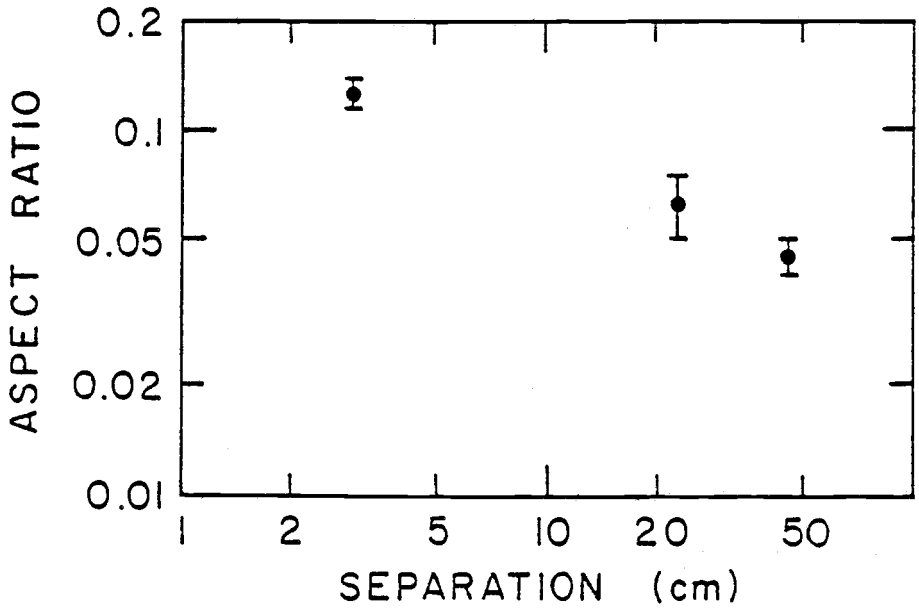

Figure V.6 Mean aspect ratio in the depth interval 20 to 50 m as a function of separation.

5. The shape of microscale features was found to vary with scale, the larger features being more flattened while the smaller ones tended toward isotropy.

6. The shape also varied strongly with vertical location (i.e. epilimnion versus thermocline) reflecting, presumably, a dependence on ambient density gradient.

Bendat, J. S. and A. G. Piersol (1971) Random Data: Analysis and Measurement Procedures. John Wiley and Sons, Inc., New York.

Birchfield, G. E. (1969) Response of a circular model Great Lake to a suddenly imposed wind stress. Journal of Geophysical Research, 74, 5547-5554.

Cairns, J. L. (1975) Internal wave measurements from a midwater float. Journal of Geophysical Research, 80, 299-306.

Caldwell, D. R. (1976) Fine-scale temperature structure in the bottom mixed layer on the Oregon shelf. Deep-Sea Research, 23, 1025-1035.

Caldwell, D. R., J. M. Brubaker and V. T. Neal (1978) Thermal microstructure on a lake slope. Limnology and Oceanography, 23, 372-374.

Caldwell, D. R., T. M. Dillon, J. M. Brubaker, P. A. Newberger, and C. A. Paulson (1979) The scaling of vertical temperature gradient spectra. (Submitted to Journal of Geophysical Research.)

Csanady, G. T. (1968) Motions in a model Great Lake due to a suddenly imposed wind. Journal of Geophysical Research, 73, 6435-6447.

Csanady, G. T. (1972) Response of large stratified lakes to wind. Journal of Physical Oceanography, 2, 3-13.

Csanady, G. T. (1975) Hydrodynamics of large lakes. Annual Review of Fluid Mechanics, 7, 357-386.

Csanady, G. T. and J. T. Scott (1974) Baroclinic coastal jets in Lake Ontario during IFYGL. Journal of Physical Oceanography, 4, 524-541.

Dillon, T. M. and T. M. Powell (1979) Observations of a surface mixed-layer. Deep-Sea Research (in press).

Eriksen, C. C. (1978) Measurements and models of fine structure, internal gravity waves, and wave breaking in the deep ocean. Journal of Geophysical Research, 83, 2989-3009.

Garrett, C. and W. Munk (1979) Internal waves in the ocean. Annual Reviews of Fluid Mechanics, 11, 339-369.

Goldman, C. R. (1970) Is the canary dying? The time has come for man, miner of the world's resources, to surface. Calif. Med., 113, 21-26.

Gregg, M. C. (1976) Finestructure and microstructure observations during the passage of a mild storm. Journal of Physical Oceanography, 6, 528-555.

Gregg, M. C. (1977) A comparison of fine-structure spectra from the main thermocline. Journal of Physical Oceanography, 7, 33-40.

Hayes, S. P. (1975) Preliminary measurements of the time-lagged coherence of vertical temperature profiles. Journal of Geophysical Research, 80, 307-311.

Hayes, S. P., T. M. Joyce, and R. C. Millard, Jr. (1975) Measurements of vertical fine structure in the Sargasso Sea. Journal of Geophysical Research, 80, 314-319.

Holland, W. R. (1977) The role of the upper ocean as a boundary layer in models of the oceanic general circulation. In: Modeling and prediction of the upper layers of the ocean. Edited by E. B. Kraus, Pergamon Press, Oxford, 7-30.

Hutchinson. G. E. (1957) A treatise on limnology. John Wiley and Sons, Inc., New York.

Kundu, P. K. (1976) An analysis of inertial oscillations observed near Oregon coast. Journal of Physical Oceanography, 6, 879-893.

Lamb, H. L. (1945) Hydrodynamics, sixth edition. Dover Publications, Inc., New York.

Lazier, J. R. N. (1973) Temporal changes in some fresh water temperature structures. Journal of Physical Oceanography, 3, 226-229.

Marmorino, G. O. and D. R. Caldwell (1978) Temperature fine structure and microstructure observations in a coastal upwelling region during a period of variable winds. Deep-Sea Research, 25, 1073-1106.

Mied, R. P. and J. P. Dugan (1975) Internal waves reflection by a layered density anomaly. Journal of Physical Oceanography, 4, 493-498.

Mortimer, C. H. (1974) Lake Hydrodynamics. Mitt. Internat. Verein. Limnol., 20, 124-197.

Nayfeh, A. H. (1973) Perturbation methods. John Wiley and Sons, Inc., New York.

Neal, V. T., S. Neshyba, and W. Denner (1969) Thermal stratification in the Arctic Ocean. Science, 166, 373-374.

Neal, V. T., S. J. Neshyba, and W. W. Denner (1971) Temperature microstructure in Crater Lake, Oregon. Limnology and Oceanography, 16, 695-700,

Otnes, R. K. and L. D. Enochson (1972) Digital time series analysis. John Wiley and Sons, Inc., New York.

Pedlosky, J. (1971) Geophysical fluid dynamics. In: Mathematical problems in the geophysical sciences, Lectures in applied mathematics, vol. 13, W. H. Reid, ed., American Mathematical Society, Providence, 1-60.

Phillips. O. M. (1977) The Dynamics of the Upper Ocean. Cambridge University Press, Cambridge.

Pinkel, R. (1975) Upper ocean internal wave observations from Flip. Journal of Geophysical Research, 80, 3892-3910.

Rao, D. B. (1966) Free gravitational oscillations in rotating rectangular basins. Journal of Fluid Mechanics, 25, 523-555.

Simpson, J. H. and J. D. Woods (1970) Temperature microstructure in a freshwater thermocline. Nature, 226, 832-835.

Smith, R. C., J. E. Tyler, and C. R. Goldman (1973) Optical properties and color of Lake Tahoe and Crater Lake. Limnology and Oceanography, 18, 189-199.

Stegen, G. R., K. Bryan, J. L. Held, and F. Ostapoff (1975) Dropped horizontal coherence based on temperature profiles in the upper thermocline. Journal of Geophysical Research, 80, 3841-3847.

Turner, J. S. (1973) Buoyancy effects in fluids. Cambridge University Press, Cambridge.

Williams, A. J. (1975) Images of ocean microstructure. Deep-Sea Research, 22, 811-830.